



Synthesis and Application of Porous and Monodispersed Silica Nano-Particles by Gradual Injection Method

メタデータ	言語: English 出版者: 公開日: 2017-01-06 キーワード (Ja): キーワード (En): 作成者: 下垣, 知代 メールアドレス: 所属:
URL	https://doi.org/10.24729/00000204

Synthesis and Application of Porous and Monodispersed
Silica Nano-Particles by Gradual Injection Method

Tomoyo Shimogaki

February 2016

Doctoral Thesis at Osaka Prefecture University

Contents

Chapter 1 General Introduction

1.1	Background; Porous Silica Materials	-----	2
1.2	Synthesis of Porous Silica Materials	-----	2
	1.2.1 Synthesis of Porous Silica Nano-Particles	-----	4
	1.2.2 Morphology Control of Porous Silica Nano-Particles	-----	4
1.3	Applications	-----	7
	1.3.1 Advanced Applications	-----	9
	1.3.2 AR Coatings	-----	11
1.4	Scope of the Present Thesis	-----	14
	References	-----	16

Chapter 2 Large- Scale Synthesis of Monodisperse Microporous Silica Nano- Particles by Gradual Injection of Reactants

2.1	Introduction	-----	22
2.2	Experimental	-----	24
	2.2.1 Materials	-----	24
	2.2.2 Synthesis	-----	24
	2.2.3 Characterization	-----	24
2.3	Results and Discussion	-----	25
	2.3.1 Optimization of Reaction Parameters	-----	25
	2.3.2 Monodisperse Porous Silica from Reaction A	-----	28
	2.3.3 Reaction Tracking	-----	32
2.4	Conclusion	-----	35
	References	-----	35

Chapter 3 Morphology Control of Microporous Silica Particles Obtained by Gradual Injection of Reactants

3.1	Introduction	-----	38
3.2	Experimental	-----	39
3.2.1	Materials	-----	39
3.2.2	Synthesis	-----	39
3.2.3	Characterization	-----	41
3.3	Results and Discussion	-----	41
3.3.1	Effect of DDA Amount (Samples 1–3)	-----	43
3.3.2	Effect of DDA Injection Time (Samples 4–6)	-----	47
3.3.3	Effect of Amount of Catalyst and Water (Samples 7–10)	-----	49
3.3.4	Effect of TMOS Concentration (Samples 11–13)	-----	50
3.4	Conclusion	-----	53
	References	-----	55

Chapter 4 Large- Scale Preparation of Morphology- Controlled Microporous Silica Particles via Gradual Injection of Reactants with Different Surfactants

4.1	Introduction	-----	58
4.2	Experimental	-----	59
4.2.1	Materials	-----	59
4.2.2	Synthesis	-----	59
4.2.3	Characterization	-----	59
4.3	Results and Discussion	-----	60
4.3.1	Ammonium Salts as Template Molecules	-----	63
4.3.2	Effect of Alkyl Chain Length	-----	65

4.3.3	Effect of Concentration of Template Amines and Reaction Time	-----	67
4.4	Conclusion	-----	71
	References	-----	71
Chapter 5 Single- Process Fabrication of Antireflective Acrylic Hard Coating via Surface Segregation of Porous Silica Nano- Particles			
5.1	Introduction	-----	76
5.2	Experimental	-----	80
5.2.1	Materials	-----	80
5.2.2	Synthesis	-----	80
5.2.3	Coating	-----	81
5.2.4	Characterization	-----	81
5.3	Results and Discussion	-----	82
5.3.1	Surface Modification	-----	82
5.3.2	Coating	-----	85
5.4	Conclusion	-----	100
	References	-----	100
Chapter 6 Conclusion			----- 103
 List of Publications			----- 107
 Acknowledgment			----- 109

Chapter 1

General Introduction

1.1 Background; Porous Silica Materials

Porous materials have been widely studied and used in many applications including medicine, electronics, optics, and environmental field, because of their characteristic porous structures. They are classified into microporous, mesoporous and macroporous materials according to porous size d ; $d \leq 2$ nm, $2 \text{ nm} < d < 50$ nm, and $d \geq 50$ nm, respectively (Fig. 1–1). Among them, micro- and mesoporous silica nano-particles have attracted huge attention in the biological fields and electric products. Especially, those of ca. 100 nm in diameter are expected to be useful for applications in cosmetics, catalysts, drug delivery systems (DDS), cell imaging and transparent media such as low-refractive index materials, thermal insulation films, and low dielectric materials. The porous silica particle is one of irreplaceable components for these applications.

1.2 Synthesis of Porous Silica Materials

A variety of porous silica has been synthesized in different processes. Kuroda and co-workers firstly succeeded in a control of pore diameter of the mesoporous material by an intercalation in 1990 [1], and reported the pore formation in 2-dimensional hexagonal structure by tuning the reaction conditions [2]. Generally, the molecular template has been used for synthesis of porous silica materials, which was first reported by reserchers in Mobil in 1992 [3]. The most common approach involves two step processing. For example, the rod-like micelle of alkyltrimethylammonium salt is used as template, and silicate or silicon alkoxide is polycondensed around the micelle. After the polycondensation, template molecules are removed by baking, to obtain the mesoporous silica called MCM-41 (Fig. 1–2). By a use of surfactant with different alkyl chain length, the pore size can be optimized for specific applications.



Fig. 1–1 Classification of microporous, mesoporous and macroporous materials according to porous size.

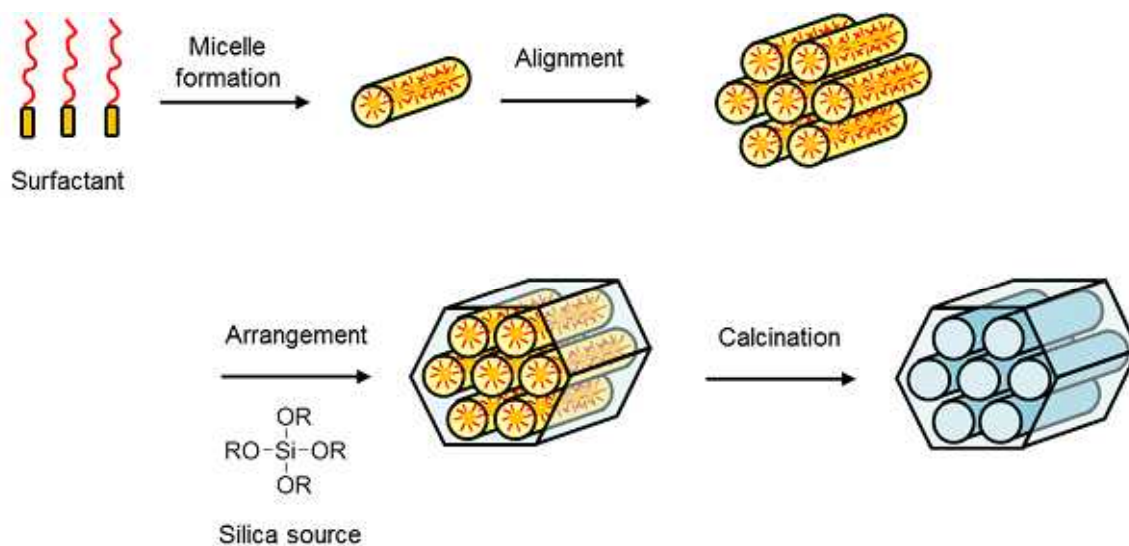


Fig. 1–2 Scheme of synthesis of porous silica [3].

1.2.1 Synthesis of Porous Silica Nano-Particles

An outstanding feature of the porous silica is that they can take a wide variety of forms such as sheet, sphere, rod and fiber. Among them, the nano-particle is expected for application in various fields and frequently studied. The porous silica nano-particles were synthesized firstly by research groups of Cai [4], Mann [5] and Osttafin [6]. Then Lai et al. popularized the term of mesoporous silica nano-particles [7]. Subsequently, the porous silica nano-particles with various morphologies were synthesized and investigated by various groups.

1.2.2 Morphology Control of Porous Silica Nano-Particles

Generally, the silica particles are synthesized by sol-gel reaction of silicon alkoxide. The hydrolysis rate of tetraalkoxy orthosilicate and the polycondensation of generated silicate are depended on many factors including pH, silica source, additives and temperature. Controlling these factors is very of critical for synthesis of porous silica particles with required properties [8].

In 1968, Stöber et al. reported a synthetic approach of monodispersed silica particles [9], which has been called “Stöber method” or “Stöber process”. In this method, the silicon alkoxide is added into reaction solution with an excess amount of water containing a little amount of alcohol and ammonia. Small silica particles with a diameter in micrometer scales could be obtained with Stöber method. Changing the reaction time and the ratio of water/silicon alkoxide, the particle size can be controlled. The alcohol/water and water/silicon alkoxide ratios of Stöber method are much larger than those of general sol-gel method. Accordingly, the reaction proceeds uniformly for producing fine particles with small variation in the particle diameter.

A variety of porous silica particles of a uniform size has been synthesized under the basic conditions with Stöber method. Using organic molecules as a template at Stöber method, the template molecules are accommodated in silica matrix. Grun et al. synthesized monodisperse mesoporous silica particles via modified Stöber method for the first time by adding a cationic surfactant to the reaction mixture [10]. Since then, a variety of synthetic approaches for monodisperse porous silica particles with different template systems has been

reported. Yano and co-workers reported the synthesis of monodisperse porous silica particles in the range of tens to a several hundred nanometers [11]. They investigated a formation mechanism of monodisperse mesoporous silica particles from the viewpoint of the particle growth and the polycondensation progress of the silica precursor. As a result, it was found that the small particles emerged suddenly at the initial stage of the synthesis, and that the residual silica precursors reacted preferentially with the surface silanols on these existing particles [11 (e)]. The more silica source was added in the presence of existing particles after the reaction, the size of the existing particles can be easily enlarged. In this case, the added silica source reacted preferentially with the surface silanol groups rather than generating new particles. This is the reason of monodisperse porous silica particles can be synthesized by the modified Stöber method.

Control of the particle diameter has been achieved through adjusting the hydrolysis and polycondensation rates of silicon alkoxide, which depend on the pH, the nature of the silicon alkoxide, concentrate and surrounding temperature [8, 12–20]. Among them, pH control is the simplest method to control the particle diameter [8, 12–17]. The hydrolysis and polycondensation rate of silicon alkoxide depend strongly on the surface charge of the reactants. In basic condition, the hydrolysis speed of silicon alkoxide becomes fast as increasing pH value (Fig. 1–3). However, the polycondensation rate is the fastest at pH = 8.4, and then decreases beyond pH = 8.4. Mou and co-workers synthesized mesoporous silica nano-particles with 30–280 nm diameters by adjusting pH from 10.86 to 11.52 [12]. They found that the particle size becomes small by decreasing pH value. They also synthesized monodisperse porous silica by separating nucleation and particles growth [13]. Quao et al. reported that the particle diameter was increased from 30 to 85 nm by decreasing pH value from 10.0 to 6.0 [16]. Chiang et al. have successfully controlled the size of mesoporous silica particle from 17 to 247 nm by controlling the amount of silicon alkoxide, reaction time, and pH value [17]. They found that the pH value is one of the most important parameters influencing particle size.

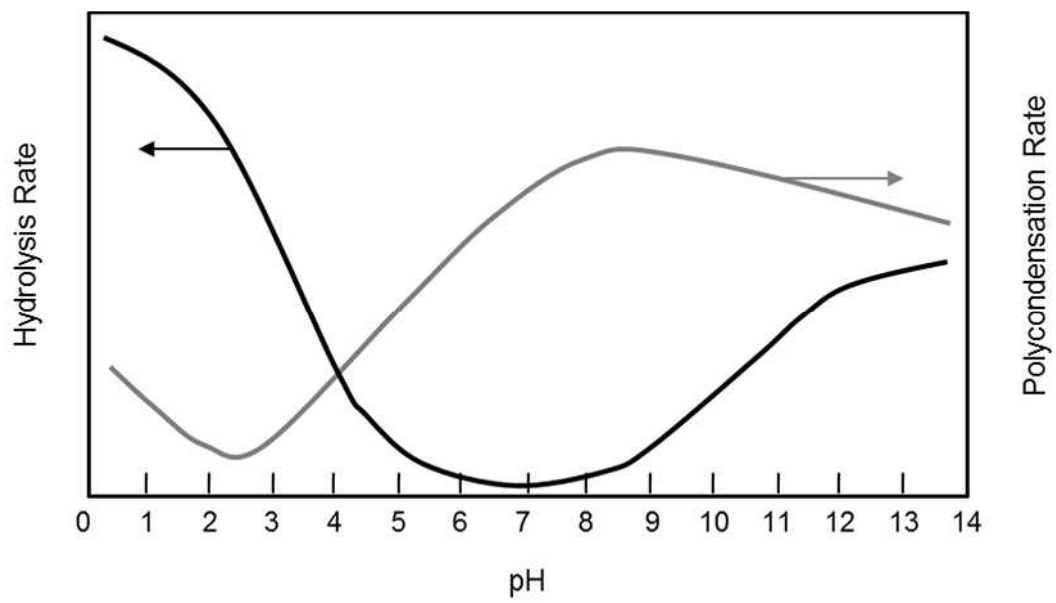


Fig. 1-3 pH dependance of hydrolysis and polycondensation rates in sol-gel reaction.

On the other hand, a kind of silicon alkoxide affects the hydrolysis rate. Kuroda's group reported that the diameter of mesoporous silica particles depends on a kind of alkoxy groups of silicon alkoxide [18]. Using the silicon alkoxide with longer alkyl chain which leads to lower hydrolysis rate, the larger particles are obtained. These results indicate that the hydrolysis and polycondensation rate are important factors for controlling particle diameter.

In addition, Nooney et al. successfully obtained spherical mesoporous silica of diameter from 65–740 nm by varying the initial silicate/surfactant ratio under dilute conditions [6]. Lin and co-workers controlled the particle size by an addition of Pluronic surfactant [19]. The formation of monodisperse mesoporous silica particles were achieved by using triblock copolymer Pluronic F127 as a particle size desiner. They found that the average size of monodisperse mesoporous silica particle can be controlled within the range of 70–500 nm depending on the amount of F127. Imai and co-workers investigated the grain size and regularity of the hexagonal array of mesoporous silica nano-particles in a binary surfactant system composed of alkylammonium chloride and Pluronic type surfactant [20]. The structure was controlled by varying the parameters for the prior hydrolysis of silicon alkoxide under an acidic condition and the subsequent assembly of silicates and surfactants under a basic condition.

1.3 Applications

The porous silica materials are widely used in many fields (Fig. 1–4). To expand the functions and applications of porous silica particles, an effect of an introduction of organic groups at the surface or framework of silica matrix is widely investigated [21–23].

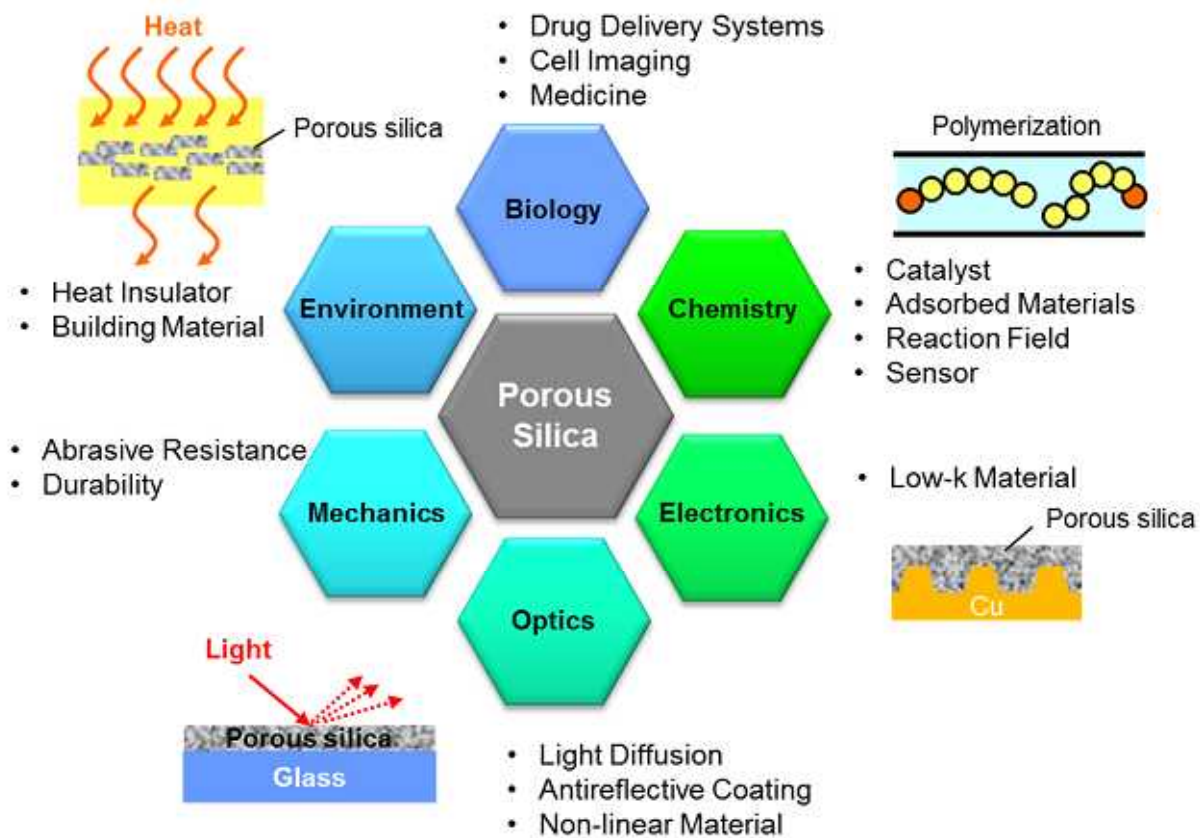


Fig. 1-4 Applications of porous silica.

There are several ways to introduce organic groups. The sol-gel reaction using organic silicon alkoxide in the presence of template molecules is one of such examples. Organic groups directly bonding to the inorganic framework can be introduced by maintaining porosity. However, there is a limit of modification density and uniformity of organic groups on the siloxane chains due to a different hydrolysis rate. Another method is post modification of porous silica particles with organic groups. Porous structure of silica particles can be maintained by the method, but the pore volume might be decreased. It is necessary to choose an appropriate way of modification depending on a purpose.

1.3.1 Advanced Applications

One of the most promised applications of the porous silica nano-particles in biomedical applications is DDS, because the mesoporous materials can act as a convenient vehicle for drugs and biomolecules [12, 24–30]. The particle size is an important factor in designing optimized DDS systems [12]. The benefit from the use of the silica particles for DDS is the thermal and chemical stability and biocompatibility. The abundant surface silanol groups can have an affinity to phospholipids which can be actively taken up by the cell [26]. Additionally, its surface can be functionalized with different molecules, which enables targeting delivery of different types of remedies. The strong Si—O bond makes silica particles more resistant to external stimuli such as mechanical stress and degradation compared to other DDS carriers such as liposomes and dendrimers. Further, the mesoporous silica particles can be also used for cell imaging for the same reasons [13, 31].

Another unique characteristics of the porous silica are low dielectric constant and low refractive index resulting from their porosity. Porous silica particles can be used as the nano-fillers to produce nanocomposite films by dispersing into the host matrix. Surface-modified porous silica particles with 20–30 nm diameters were coated on various substrates as a layer antireflective (AR) coating [32, 33] (Fig. 1–5). By adjusting the thickness (around 100–150 nm) and porosity of the mesoporous silica, an excellent AR property in the visible wavelength range has been achieved. Thus, it is greatly important to control the morphology of porous silica particles for these applications.

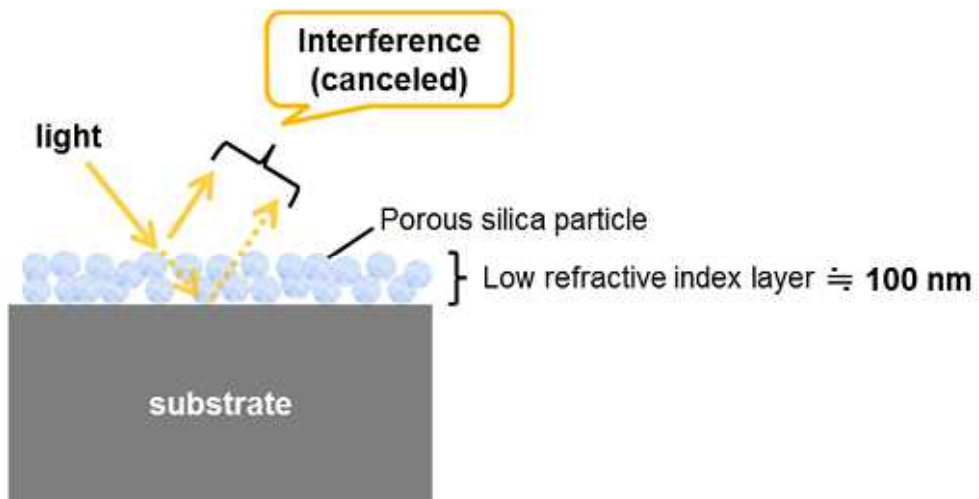


Fig. 1-5 Concept of AR coating [32].

1.3.2 AR Coatings

AR coatings are an important class of technology used to improve the quality of our daily life by offering a better visibility for flat panel displays, mobile phones and tablets by reducing the reflection of surrounding light [34–36]. Two types of AR coating have been reported and industrialized so far. One is the moth's eye structure, which mimics the eyes of moths, in which micro cones ~100 nm in diameter and several hundreds of nm in height with 100 to 200 nm regular spacing are fabricated on the entire surface of the display devices [37–43] (Fig. 1–6). The refractive index of the moth's eye surfaces gradually changes from that of air to that of the window material. The optical reflection is suppressed because of the absence of a refractive index jump at the interface. Such structure shows an excellent AR capability. However, the sophisticated lithographic technique at the 100 nm scale is required to fabricate the moth's eye structure. In addition, such micro structures are very fragile and do not survive mechanical contact by human fingers or other objects. Furthermore, the substrate is limited to hard materials such as glasses because they need to be capable of nanolithography. Further improvement in mechanical robustness is strongly required for moth's eye-structured AR surfaces.

Another type of AR coating is multilayer optical thin films, which is designed to cancel the optical reflection by optical interference within the multilayers of alternating refractive indexes [44–46] (Fig. 1–7). Such thin film is widely used for displays or glasses presently available because of their simple structure and better surface mechanical properties. By preparing an optical thin film with a designated refractive index and thickness, the two reflections at the air/film and film/device interfaces interfere each other, resulting in the cancelation of the reflection of light through an anti-phase interaction. Low-refractive index coatings are usually required for this type of AR coating. However, the low refractive index layer is required to be coated at a thickness of 100 nm with an accuracy of several nanometers, which is technologically very difficult from an industrial point of view. Therefore, an easier and simpler method for robust AR coatings is strongly required from both industrial and practical points of view.

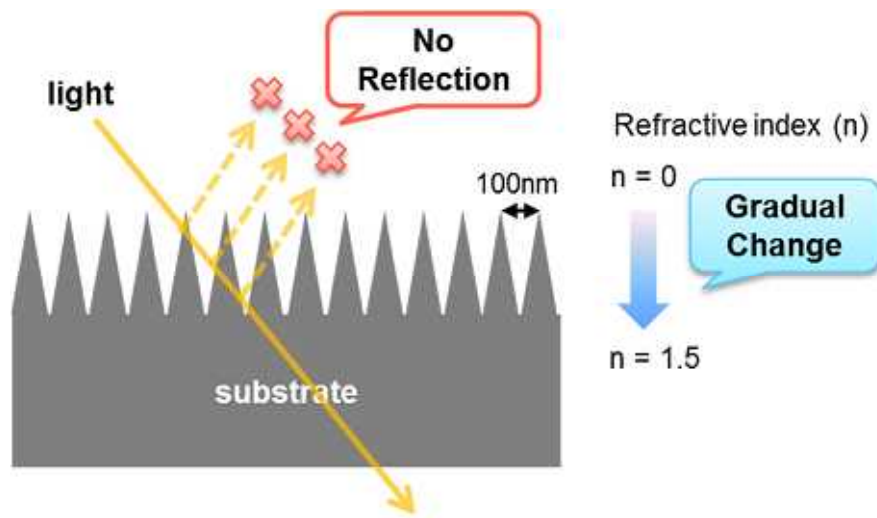


Fig. 1-6 Moth's eye structure.

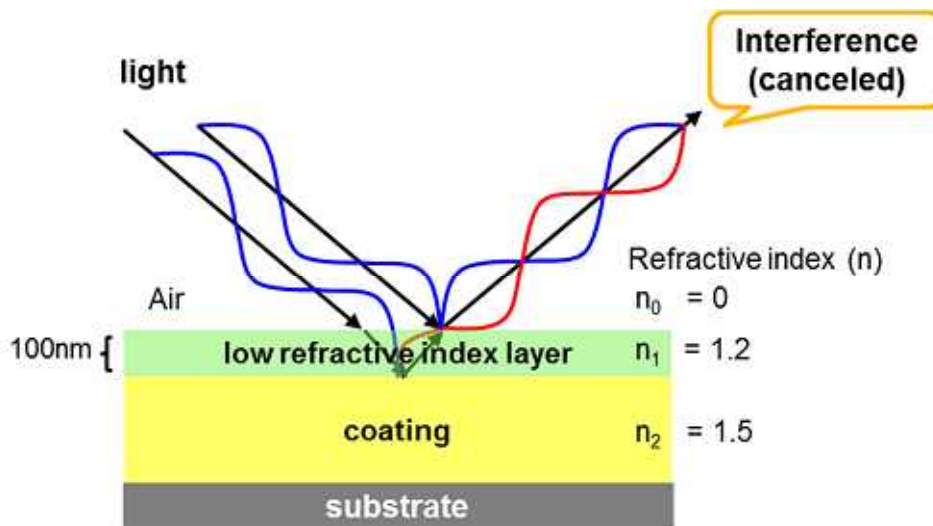


Fig. 1-7 Multilayer type structure.

1.4 Scope of the Present Thesis

This thesis deals with a development of new synthesis method of fine-tuned microporous silica particles with industrial scale and proposes a new application for an AR coating using these microporous silica particles. The gradual injection method in which reactants are injected in the reaction field to keep reactive silicon alkoxide dilute concentration has been proposed, which can suppress the drastic reaction and the generation of aggregated large silica particles. Furthermore, the AR coating using synthesized porous silica particles with simple wet process was developed.

A hard coating acrylic polymer film with a surface-segregated porous silica nano-particle layer has been proposed as a new type of AR coating possessing mechanical robustness coupled with excellent optical quality used porous silica particle as low refractive index material with easily coating process. The surface porous silica layer serves as a surface low-refractive index layer that does not deteriorate and demonstrates the mechanical robustness of a polymer hard coating. One of the advantages of the present approach is that the substrate materials are not limited, which means they can be used for variety of applications. In addition, such composite films can be formed via a single coating process. The surface porous silica particle layer is formed through spontaneous self-organization during the coating process.

To achieve the proposed AR coating system, control of morphology and efficient produce of silica particles are of significant. The monodispersed silica particles with 10-150 nm in diameter are very useful as filler for transparent materials because the visible light is not scattered by these particles. Although there have been many reports on the synthesis of monodisperse porous silica nano-particles with such diameter, the fundamental problem of those synthetic condition is concentration of the system which is usually too dilute to produce on an industrial scale. So far, researches on the large scale production of monodisperse porous silica are quite few. For example, the silicon alkoxide concentration in general synthesis of monodisperse porous silica particle with ca. 100 nm in diameter is less than 0.5 wt.% [6, 11, 18 (b)]. The molecular weight of silicon alkoxide is decreased to half by undergoing hydrolysis. This indicated that the silica particles can be obtained only 2.5 g at most on the synthetic scale of 1 L, which is not enough efficient for commercial applications. The large scale synthetic with

condensed system is urgently required. Then, I tried to establish the synthesis procedure of monodisperse porous silica nano-particles with $>500 \text{ m}^2/\text{g}$ in specific surface area (SSA) and 100 nm in diameter in yield 10 times more than existing methods.

This thesis consists of six chapters.

Chapter 1 is general introduction. The background in this field and the scope of this thesis are described.

In Chapter 2, < Large-Scale Synthesis of Monodisperse Microporous Silica Nano-Particles by Gradual Injection of Reactants >, the monodisperse microporous silica particles were synthesized with high yield by the gradual injection of tetramethoxy orthosilicate and template molecules into the reaction system. The monomer and other reactants were supplied continuously, ensuring a constant concentration of silicon alkoxide and template molecules in the reaction system. The production of monodisperse porous silica nano-particles in high yield is possible with the present approach.

In Chapter 3, < Morphology Control of Microporous Silica Particles Obtained by Gradual Injection of Reactants >, the relationship between the synthetic parameters and morphologies of the resulting silica particles were investigated. The influence of injection kinetics and amount of template molecules and catalyst on the particle morphology was investigated. Their SSA could be tuned from 100 to $500 \text{ m}^2/\text{g}$ by the amount of templating molecule, n-dodecylamine, without changing the particle size and dispersibility.

In Chapter 4, < Large-Scale Preparation of Morphology-Controlled Microporous Silica Particles via Gradual Injection of Reactants with Different Surfactants >, the influence of species of template molecules on the particle morphology was investigated. The relationship between obtained particle morphology and solubility in reaction solutions was revealed. The synthesis of the porous silica particles with a large pore volume and monodispersibility via gradual injection method were achieved. These results show that the gradual injection of the reactants in a controlled manner is effective to the industrial-scale synthesis of the silica nano-particles with expected morphologies.

In Chapter 5, < Single-Process Fabrication of Antireflective Acrylic Hard Coating via

Surface Segregation of Porous Silica Nano-Particles >, a new type of AR coating using porous silica nano-particles as low refractive index materials is proposed. This AR coating consists of a surface-segregated single layer of silica nano-particles and acrylic polymer matrix and proposed that exhibits good mechanical stability and AR capability. In addition, the polymer hard coating can be obtained by a single coating process. The mechanism of forming AR coating and its performance were verified.

Finally, conclusion of this thesis is described in Chapter 6.

References

1. (a) T. Yanagisawa, T. Shimizu, K. Kuroda and C. Kato, *Bull. Chem. Soc. Jpn.*, 1990, **63**, 988–992. (b) T. Yanagisawa, T. Shimizu, K. Kuroda and C. Kato, *Bull. Chem. Soc. Jpn.*, 1990, **63**, 1535–1537.
2. S. Inagaki, T. Fukushima and K. Kuroda, *J. Chem. Soc, Chem. Commun.*, 1993, **8**, 680–682.
3. (a) C. T. Kresge, M. E. Leonowicz, W. J. Roth, J. C. Vartuli and J. S. Beck, *Nature*, 1992, **359**, 710–712. (b) J. S. Beck, J. C. Vartuli, W. J. Roth, M. E. Leonowicz, C. T. Kresge, K. D. Schmitt, C. T. -W. Chu, D. H. Olson, E. W. Sheppard, S. B. McCullen, J. B. Higgins and J. L. Schlenker, *J. Am. Chem. Soc.*, 1992, **114**, 10834–10843.
4. Q. Cai, Z. S. Luo, W. Q. Pang, Y. W. Fan, X. H. Chen and F. Z. Cui, *Chem. Mater.*, 2001, **13**, 258–263.
5. C. E. Fowler, D. Khushalani, B. Lebeau and S. Mann, *Adv. Mater.*, 2001, **13**, 649–652.
6. R. I. Nooney, D. Thirunavukkarasu, Y. M. Chen, R. Josephs and A. E. Ostafin, *Chem. Mater.*, 2002, **14**, 4721–4728.
7. C. Y. Lai, B. G. Trewyn, D. M. Jeftinija, K. Jeftinija, S. Xu, S. Jeftinija and V. S. Y. Lin, *J. Am. Chem. Soc.*, 2003, **125**, 4451–4459.
8. C. J. Brinker and G. W. Scherer, *Sol-Gel Science: The Physics and Chemistry of Sol-Gel Processing*; Academic Press: Boston, 1990.
9. W. Stöber and A. Fink, *J. Colloid Interface Sci.*, 1968, **26**, 62–69.

10. M. Grün, I. Lauer and K. K. Unger, *Adv. Mater.*, 1997, **9**, 254–256.
11. (a) K. Yano, N. Suzuki, Y. Akimoto and Y. Fukushima, *Bull. Chem. Soc. Jpn.*, 2002, **75**, 1977–1082. (b) K. Yano and Y. Fukushima, *J. Mater. Chem.*, 2003, **13**, 2577–2581. (c) K. Yano and Y. Fukushima, *J. Mater. Chem.*, 2004, **14**, 1579–1584. (d) Y. Yamada and K. Yano, *Micro. Meso. Mater.*, 2006, **93**, 190–198. (e) T. Nakamura, M. Mizutani, H. Nozaki, N. Suzuki and K. Yano, *J. Phys. Chem. C.*, 2007, **111**, 1093–1100. (f) M. Mizutani, Y. Yamada, T. Nakamura and K. Yano, *Chem. Mater.*, 2008, **20**, 4777–4782. (g) K. Yano, M. B. Katz, X. Pan and N. Tatsuda, *J. Colloid. Interface Sci.*, 2014, **418**, 61–65.
12. F. Lu, S.-H. Wu, Y. Hung and C.-Y. Mou, *Small*, 2009, **5**, 1408–1413.
13. Y.-S. Lin, C.-P. Tsai, H.-Y. Huang, C.-T. Kuo, Y. Hung, D.-M. Huang, Y.-C. Chen and C.-Y. Mou, *Chem. Mater.*, 2005, **17**, 4570–4573.
14. V. K. Lamer and R. H. Dinegar, *J. Am. Chem. Soc.*, 1950, **72**, 4847–4854.
15. S. -H. Wu, C. -Y. Mou and H. -P. Lin, *Chem. Soc. Rev.*, 2013, **42**(9), 3862–3875.
16. Z.-A. Qiao, L. Zhang, M. Guo, Y. Liu, and Q. Huo, *Chem. Mater.*, 2009, **21**, 3823–3829.
17. Y.-D. Chiang, H.-Y. Lian, S.-Y. Leo, S.-G. Wang, Y. Yamauchi and K. C.-W. Wu, *J. Phys. Chem. C*, 2011, **115**, 13158–13165.
18. (a) C. Urata, Y. Aoyama, A. Tonegawa, Y. Yamauchi and K. Kuroda, *Chem., Commun.*, 2009, 5094–5096. (b) H. Yamada, C. Urata, Y. Aoyama, S. Osada, Y. Yamauchi and K. Kuroda, *Chem. Mater.*, 2012, **24**, 1462–1471. (c) H. Yamada, C. Urata, H. Ujiie, Y. Yamauchi and K. Kuroda, *Nanoscale*, 2013, **5**, 6145–6153.
19. T.-W. Kim, P.-W. Chung and V. S.-Y. Lin, *Chem. Mater.*, 2010, **22**, 5093–5104.
20. (a) K. Suzuki, K. Ikari and H. Imai, *J. Am. Chem. Soc.*, 2004, **126**, 462–463. (b) K. Ikari, K. Suzuki and H. Imai, *Langmuir*, 2006, **22**, 802–806.
21. A. Stein, B. J. Melde and R. C. Schroden, *Adv. Mater.*, 2000, **12**, 1403–1419.
22. F. Hoffmann, M. Cornelius, J. Morell and M. Fröba, *Angew. Chem. Int. Ed.*, 2006, **45**, 3216–3251.
23. F. Hoffmann and M. Fröba, *Chem. Soc. Rev.*, 2011, **40**, 608–620.
24. C. Barbé, J. Bartlett, L. Kong, K. Finnie, H. Q. Lin, M. Larkin, S. Calleja, A. Bush and G. Calleja, *Adv. Mater.*, 2004, **16**, 1959–1966.

25. J. Lu, M. Liong, J. I. Zink and Fu. Tamanoi, *Small*, 2007, **3** (8), 1341–1346.
26. M. Liong, J. Lu, M. Kovoichich, T. Xia, S. G. Ruehm, A. E. Nel, F. Tamanoi and J. I. Zink, *ACS Nano*, 2008, **2** (5), 889–896.
27. X. Du and J. He, *Nanoscale*, 2011, **3**, 3984–4002.
28. Y.-S. Lin, K. R. Hurley and C. L. Haynes, *J. Phys. Chem. Lett.*, 2012, **3**, 364–374.
29. P. Yang, S. Gaib and J. Lin, *Chem. Soc. Rev.*, 2012, **41**, 3679–3698.
30. S. Kwon, R. K. Singh, R. A. Perez, E. A. A. Neel, H.-W. Kim and W. Chrzanowski, *J. Tissue Eng.*, 2013, **4**, 1–18.
31. (a) M. Nakamura and K. Ishimura, *Langmuir*, 2008, **24**, 12228–12234. (b) M. Nakamura, M. Shono and K. Ishimura, *Anal. Chem.*, 2007, **79**, 6507–6514. (c) M. Nakamura, S. Ozaki, M. Abe, T. Matsumoto and K. Ishimura, *J. Mater. Chem.*, 2011, **21**, 4689–4695.
32. Y. Hoshikawa, H. Yabe, A. Nomura, T. Yamaki, A. Shimojima and T. Okubo, *Chem. Mater.*, 2010, **22**, 12–14.
33. J. Moghal, J. Kobler, J. Sauer, J. Best, M. Gardener, A.A.R. Watt and G. Wakefield, *ACS Appl. Mater. Interfaces*, 2012, **4**, 854–859.
34. M. Ibn-Elhaj and M. Schadt, *Nature*, 2001, **410**, 796–799.
35. H. K. Raut, V. A. Ganesh, A. S. Nair and S. Ramakrishna, *Energy Environ. Sci.*, 2011, **3**, 3779–3804.
36. G. S. Lim, H. Kim and J. Y. Chang, *J. Mater. Chem. C*, 2014, **2**, 10184–10188.
37. P. B. Clapham and M. C. Hutley, *Nature*, 1973, **244**, 281–282.
38. J. Nishii, K. Kintaka, Y. Kawamoto, A. Mizutani and H. Kikuta, *J. Ceram. Soc. Jpn.*, 2003, **111**, 24–27.
39. Y. Li, J. Zhang, S. Zhu, H. Dong, F. Jia, Z. Wang, Z. Sun, L. Zhang, Y. Li, H. Li, X. Xu and B. Yang, *Adv. Mater.*, 2009, **21**, 4731–4734.
40. Y. Li, J. Zhang and B. Yang, *Nano Today*, 2010, **5**, 117–127.
41. S. Chattopadhyay, Y. F. Huang, Y. J. Jen, A. Ganguly, K. H. Chen and L. C. Chen, *Materials Science and Engineering R*, 2010, **69**, 1–35.
42. H. Deniz, T. Khudiyev, F. Buyukserin and M. Bayindir, *Appl. Phys. Lett.*, 2011, **99**, 183107.
43. S. Kim, U. T. Jung, S. -K. Kim, J. -H. Lee, H. S. Choi, C. -S. Kim and M. Y. Jeong, *ACS*

- Appl. Mater. Interfaces*, 2015, **7**, 326–331.
44. J. A. Hiller, J. D. Mendelsohn and M. F. Rubner, *Nat. Mater.*, 2002, **1**, 59–63.
45. S. Kim, J. Cho and K. Char, *Langmuir*, 2007, **23**, 6737–6743.
46. Y. Du, L. E. Luna, W. S. Tan, M. F. Rubner and R. E. Cohen, *ACS Nano*, 2010, **4**, 4308–4316.

Chapter 2

Large- Scale Synthesis of Monodisperse Microporous Silica Nano- Particles by Gradual Injection of Reactants

2.1 Introduction

Nano- and mesoporous silica materials have applications in catalysis, adsorption, and optical devices. Particles with diameters around 100 nm are attractive transparent materials, because of their large surface areas (which can exceed several hundred m^2/g) and negligible light scattering. The Stöber method is commonly used to prepare monodispersed silica particles [1]. This involves the hydrolysis of silicon alkoxide in a closed vessel under basic conditions. Preparing monodisperse mesoporous silica by a modified Stöber method using template organic molecules such as alkyl amines and ammonium salts has been achieved [2–14]. The most common approach involves two steps. Micro- and mesostructures are first introduced by accommodating template agents in the silica matrix. The subsequent removal of the template leaves nano- or mesopores in the silica matrix. Pore characteristics can be optimized for specific applications, by selecting a suitable template and optimizing the processing conditions.

Control of the particle diameter has been achieved through the hydrolysis and polycondensation rates of silicon alkoxide, which depend on the pH, the nature of the silicon alkoxide and surrounding temperature [2, 4, 7–9, 14–20]. There have been several reports on the synthesis of porous silica particles with diameters around 100 nm [6, 9, 13–21], but few have achieved a narrow particle size distribution. The reported methods also involve low yields and long reaction times, so are unsatisfactory for industrial application. A high reactant concentration is generally required for efficient production, but this causes particle condensation and aggregation, the growth of secondary particles, and an increase in the particle size distribution. Obtaining monodisperse porous silica particles from high concentration solutions for large-scale production remains difficult. It is also difficult to control the pH of systems containing alkyl amines or alkyl ammonium salts, and thus the hydrolysis and condensation rates. An efficient straight-forward process for the large-scale production of 100 nm monodisperse porous silica is required [21].

I report the synthesis of monodisperse porous silica particles of size 100–130 nm in high yield. The monomer and other reactants were supplied continuously, ensuring a constant concentration of silicon alkoxide and template molecules in the reaction system. This resulted in the production of monodisperse porous silica nano-particles in high yield (Fig. 2–1).

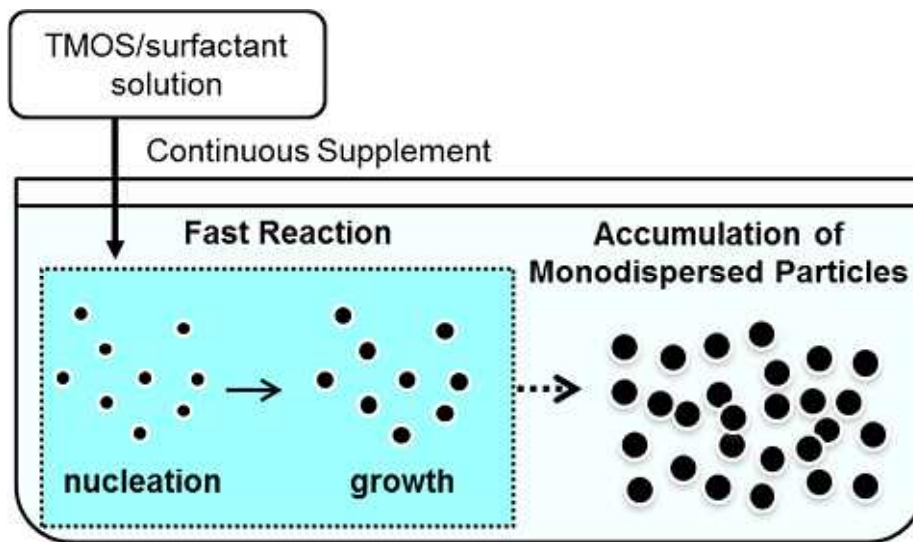


Fig. 2-1 Schematic diagram of the present processing; gradual injection of silicon alkoxide into reaction chamber.

2.2 Experimental

2.2.1 Materials

Methanol (Kanto Chemical Co. Inc., Japan), tetramethoxy orthosilicate (TMOS; Shin-Etsu, Japan), n-dodecylamine (DDA; TCI, Japan), and 28 % aqueous solution of NH₃ (Wako Inc., Japan) were used as received.

2.2.2 Synthesis

(a) Reaction A

Methanol (852.8 g), distilled water (245.2 g) and 28 % aqueous solution of NH₃ (109.6 g) were mixed in a 2 L four-neck flask at 20 °C. Methanol (180.4 g), DDA (37.1 g) and TMOS (137.2 g) were mixed in polyethylene (PE) container, which were then injected into the flask with a tube pump for 120 min under vigorous stirring. The molar ratio for the conclusive reaction solution was TMOS/DDA/NH₃/H₂O = 0.5/0.1/1/10. The reaction solution was stirred for another 1 h. The resulting precipitates were collected by centrifugation and dried at 120 °C in air for 2 h, and calcined in air at 600 °C for 6 h to remove DDA. (yield: 48.9 g)

(b) Reaction B

DDA (9.3 g), methanol (213.2 g), distilled water (61.3 g), and 28 % aqueous solution of NH₃ (27.4 g) were mixed in a 500 mL four-neck flask at 20 °C. Methanol (45.1 g) and TMOS (34.3 g) were mixed in PE container, which were then injected into the flask with a tube pump for 120 min under vigorous stirring. The molar ratio for the conclusive reaction solution was TMOS/DDA/NH₃/H₂O = 0.5/0.1/1/10. The reaction solution was stirred for another 1 h. The resulting precipitates were collected by centrifugation and dried at 120 °C in air for 2 h, and calcined in air at 600 °C for 6 h to remove DDA. (yield: 12.0 g)

2.2.3 Characterization

Scanning electron microscope (SEM) images were obtained using a JSM-7500TFE microscope (JEOL Ltd., Japan), at an accelerating voltage of 0.5 kV. Transmission electron microscope (TEM) images were obtained using a JEM-2200FS microscope (JEOL Ltd.), at an

accelerating voltage of 200 kV. Dynamic light scattering (DLS) measurements were recorded using a Zetasizer Nano ZS instrument (Malvern, U.K.). Specific surface areas (SSA) values were determined by the Brunauer Emmett Teller (BET) method, using a SA-6200 instrument (Horiba, Japan). N₂ adsorption-desorption isotherms were obtained at 77 K using a BELSORP-max instrument (BEL Japan Inc., Japan). Samples were pretreated at 373 K for 5 h and then at 473 K for 5 h in a vacuum deaeration. Pore size distributions were calculated using MP methods. Small angle X-ray scattering patterns were obtained using a Rint-TTR II diffractometer (Rigaku, Japan) with Cu K α radiation.

2.3 Results and Discussion

2.3.1 Optimization of Reaction Parameters

A dilute reactant concentration is necessary for suppressing aggregation of the silica nano-particles. Thus, the supply of the silicon alkoxide silica source was regulated, by its slow injection into the reaction system. TMOS was used as the silica source to prepare small particles, because of its fast hydrolysis. TMOS was injected over 120 min into a basic aqueous solution containing methanol, water, and ammonia. DDA was used as the template molecule. The effect of DDA on the morphology of the silica particles was examined by comparing two different injection procedures, as shown in Fig. 2-2 (a) and (b). Reaction A involved injecting DDA and TMOS into the basic aqueous solution. On the other hand, reaction B involved injecting solely TMOS into the basic aqueous solution dissolving DDA in advance. After reaction, the white powder was collected by centrifugation and dried at 393 K for 2 h, and baked in air at 873 K for 6 h to remove DDA.

SEM images of particles prepared from reactions A and B are shown in Fig. 2-3 (a) and (b), respectively. Particles from reaction A exhibited similar diameters of 100–130 nm, but the diameters of those from reaction B were larger and more diverse. It should be noticed that monodispersed mesoporous silica of <150 nm in diameter could be obtained by the present protocol.

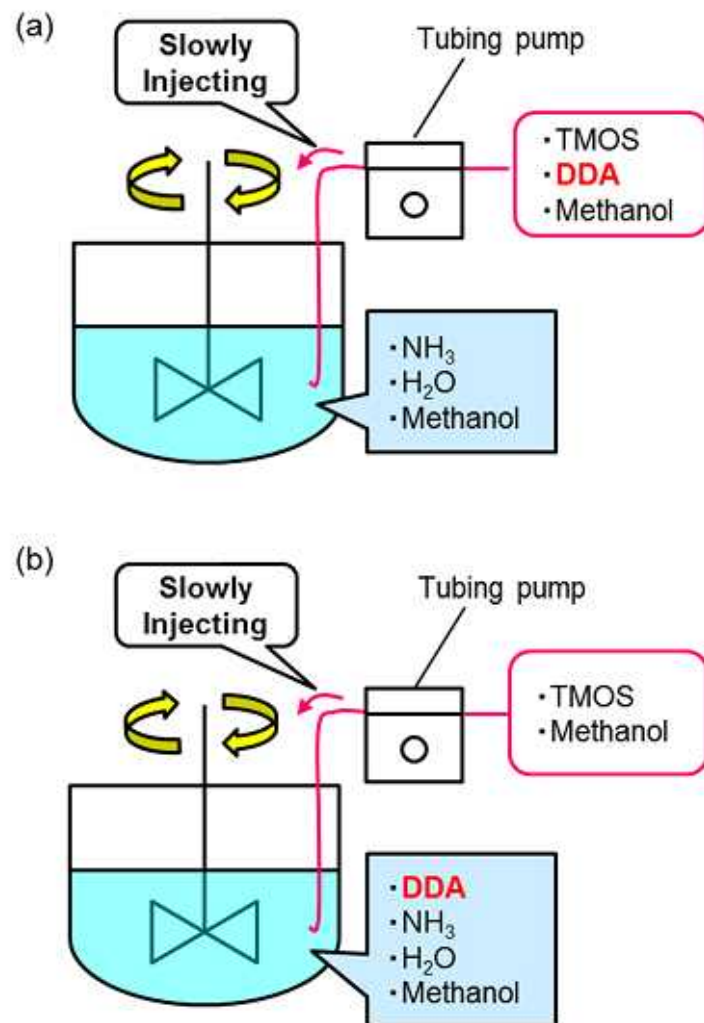


Fig. 2-2 Schematic of synthesis porous silica with reaction (a) A and (b) B: (a) injecting DDA gradually with TMOS and (b) DDA initially incorporating in reaction solution.

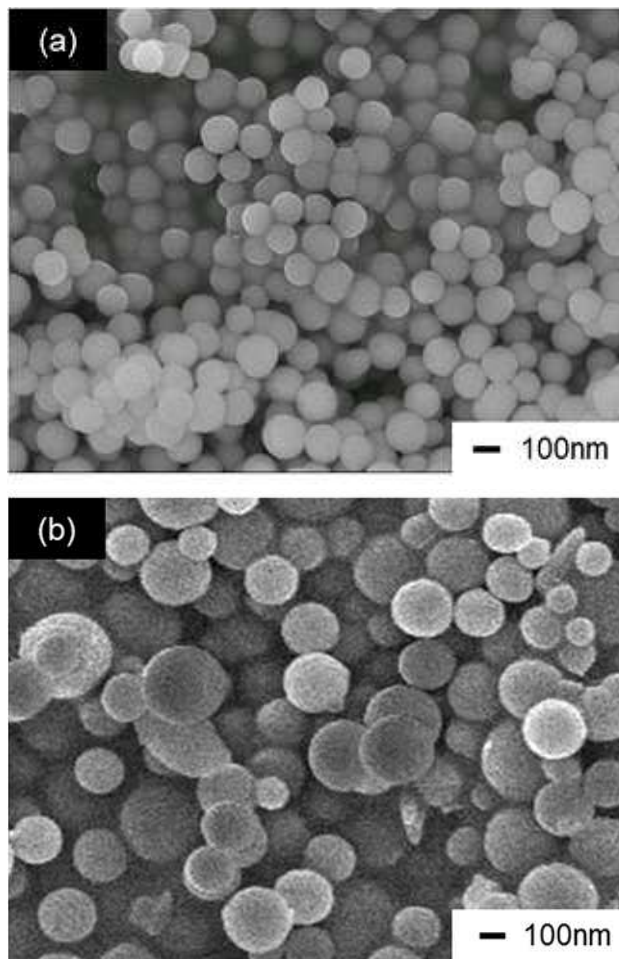


Fig. 2-3 SEM images of porous silica particles from reaction (a) A and (b) B.

Fig. 2–4 shows a TEM image of a silica particle from reaction A, in which micropores were oriented approximately radially. The BET surface areas of particles from reactions A and B were 130 and 710 m²/g, respectively. This indicated that the simultaneous injection of TMOS and DDA into the reaction system was effective for preparing monodisperse porous silica particles. Monodisperse porous silica particles were obtained in high yield, using a silicon alkoxide concentration of 9.0 wt.%. The scale-up should be easier than in the other modified Stöber method, because of the simplicity of the process. A 5 L reaction volume was undertaken in our laboratory. Modified Stöber methods involve typical silicon alkoxide concentrations of under 1 wt.% [6, 9, 13, 15–17]. It is difficult to obtain monodispersed silica particles of diameters <150 nm from such concentrations.

2.3.2 Monodisperse Porous Silica from Reaction A

The pore size and volume of the silica particles from reaction A were measured to be 0.9 nm and 0.04 cm³/g, respectively, as shown in Fig. 2–5. No peak at 2–3° in 2 θ was observed in the X-ray diffraction pattern in Fig. 2–6, indicating that the pores were randomly orientated. This indicated that the DDA template was incorporated not as micelles, but as free molecules in the interstices of siloxane molecules. Previous reports of the modified Stöber method involved a tetraethoxy orthosilicate (TEOS) silica source and DDA template and catalyst [4, 5], which yielded monodisperse porous silica particles of 0.4–1.2 μ m in diameter and 3.1 nm in pore size. In that case [4, 5] the templating agent was incorporated as irregularly arranged micelles because the pore size is estimated as 3.1 nm. The interaction of DDA with TEOS was weaker than that with TMOS, because the hydrolysis rate of TEOS was slower than that of TMOS.

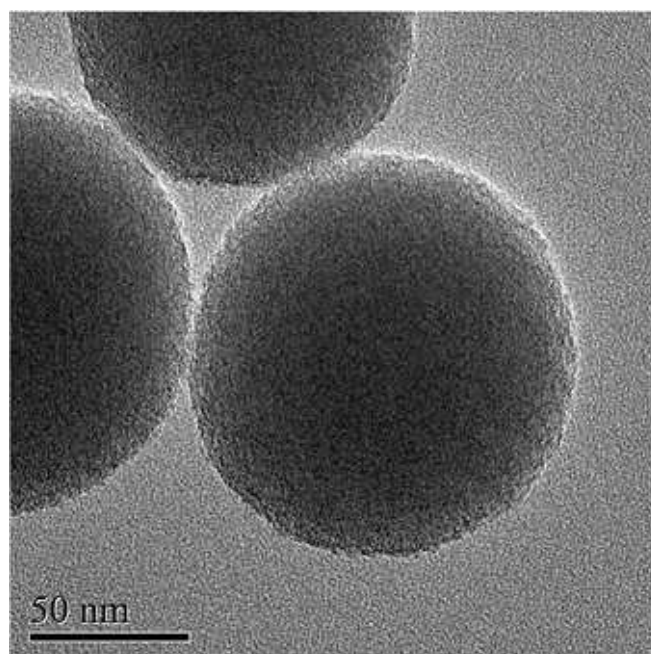


Fig. 2-4 TEM image of silica particles obtained from reaction A.

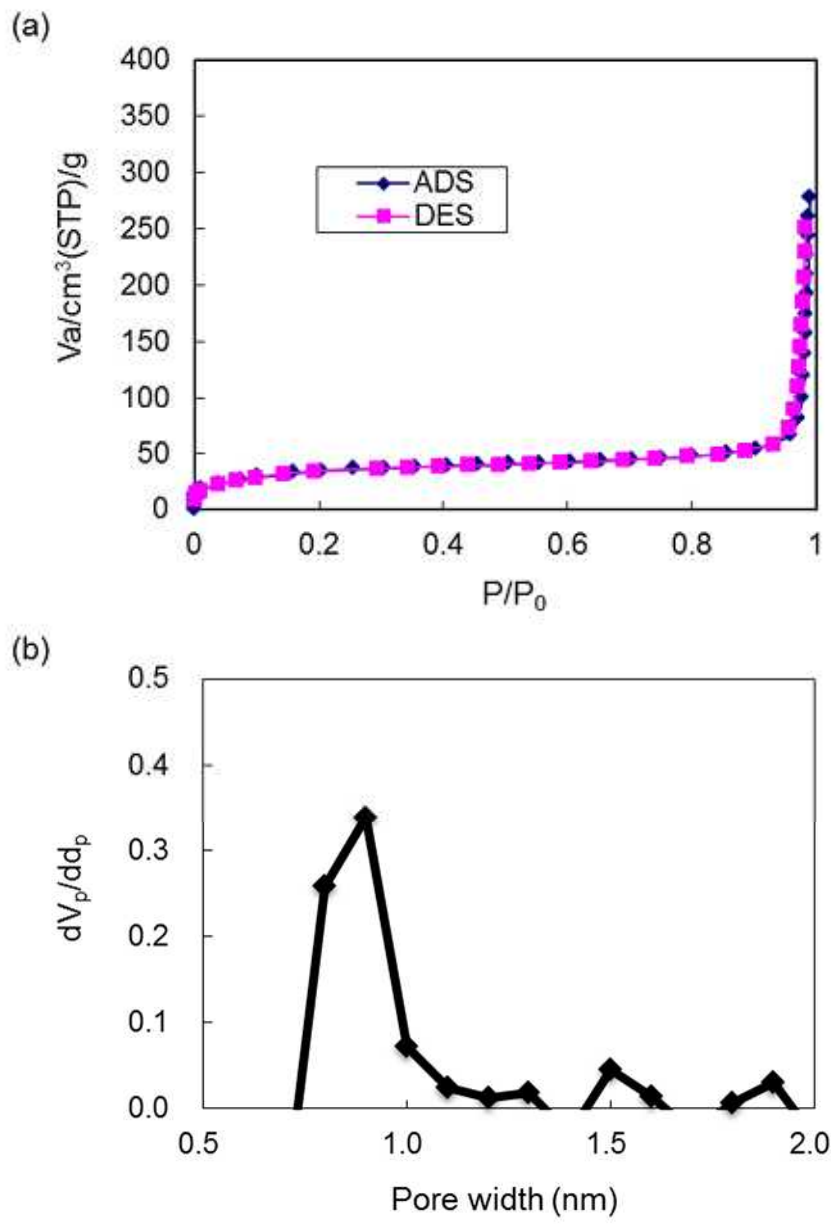


Fig. 2-5 (a) Nitrogen adsorption-desorption isotherms of obtained silica by reaction A and (b) pore size distribution curves from MP method.

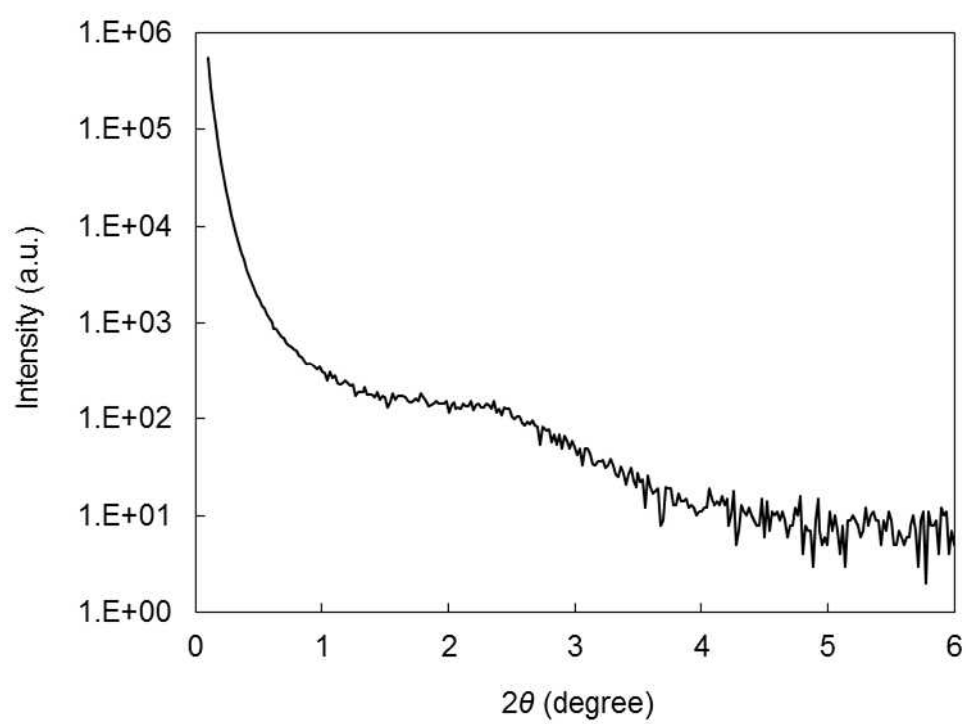


Fig. 2–6 Small angle X-ray scattering pattern for obtained silica porous by reaction A.

2.3.3 Reaction Tracking

Particle size distributions and SEM images were observed at prescribed time intervals, to trace the change in particle morphology and to observe the particle growth process (Figs. 2–7 and 2–8). Aliquots of reaction mixture were collected at regular time intervals. The particle size distribution curve maximum shifted toward larger diameter with increasing reaction time. The average particle size was ~170 nm (this value was estimated by DLS) after a reaction time of 100 min, at which point the particle growth exhibited saturation. This indicated that larger particles grew more slowly than smaller particles, because smaller particles had larger SSA and therefore more TMOS reaction sites. The particle size distribution narrowed in the later stages of reaction, despite the continuous nucleation occurring during TMOS injection (Fig. 2–1).

In the modified Stöber method, TMOS is mixed with other reagents at the beginning of reaction, and nucleation occurs only during the early stage of the process. Nucleation is too fast to yield small monodispersed particles, when using initial TMOS concentrations as high as that in the present process. In the present study, nucleation occurred at dilute TMOS concentration. In reaction A, 0.5 M TMOS yielded porous particles in 30–40 wt.%, relative to the TMOS source.

The modified Stöber method [4, 5] can yield monodispersed silica particles, but only of size much larger than those of reaction A. This is despite the total silicon alkoxide concentration being lower than that used in the current system. The TMOS concentration remained dilute until hydrolysis and polycondensation occurred, so aggregation was suppressed. This process is useful for synthesizing silica particles in high yield.

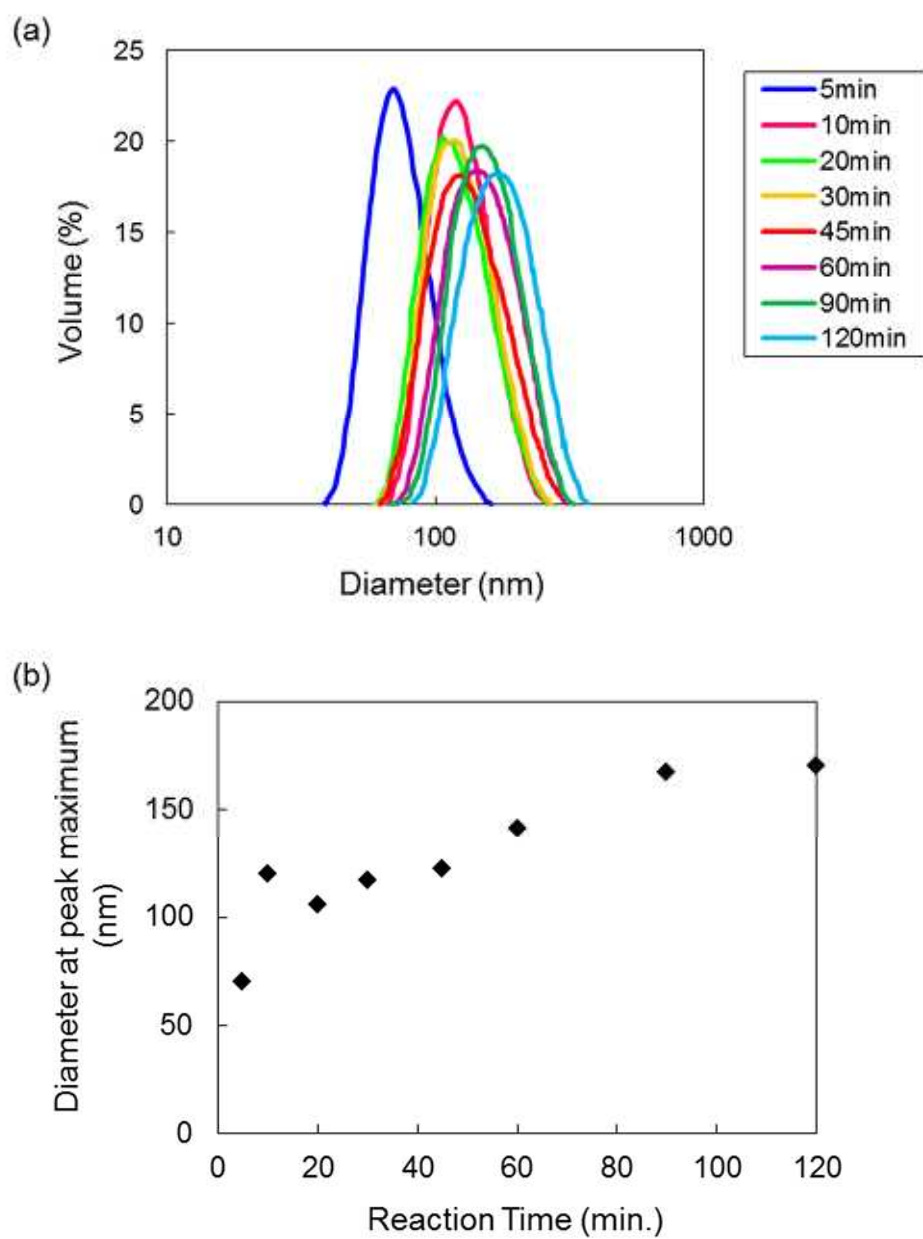


Fig. 2-7 Variation in (a) particle size distribution and (b) particle size distribution curve maximum with increasing reaction time (5–120 min).

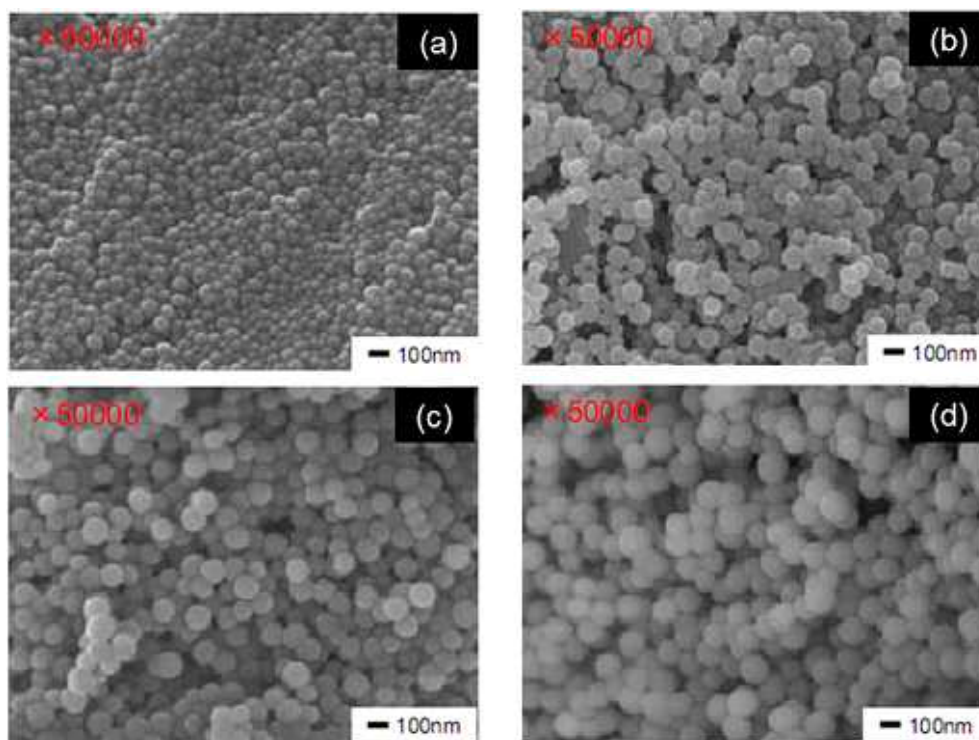


Fig. 2-8 SEM images of porous silica particles prepared after reaction times of (a) 10, (b) 30, (c) 60 and (d) 120 min.

2.4. Conclusion

Monodisperse porous silica particles with diameters of ~150 nm were prepared in high yield. The simultaneous injection of TMOS and DDA achieved the same rate to keep same conversion of substrates. The gradual supply of TMOS was important for controlling the particle morphology. This method is also applicable for synthesizing small silica particles using other template molecules.

References

1. W. Stöber and A. Fink, *J. Colloid Interface Sci.*, 1968, **26**, 62–69.
2. K. K. Unger, G. Kreysa and J. P. Baselt (Eds.), *Characterisation of Elsevier*, Amsterdam, 2000.
3. K. K. Unger, D. Kumar, M. Grün, G. Büchel, S. Lüdtke, Th. Adam, K. Schumacher and S. Renker, *J. Chromatogr. A*, 2000, **892**, 47–55.
4. Y. Shiratori, H. Saito, M. Higuchi, K. Katayama and Y. Azuma, *J. Ceram. Soc. Japan*, 2002, **110**, 304–309.
5. Y. Shiratori, H. Saito, M. Higuchi, T. Asaka, K. Katayama and Y. Azuma, *J. Ceram. Soc. Japan*, 2003, **111**, 104–109.
6. K. Yano, N. Suzuki, Y. Akimoto and Y. Fukushima, *Bull. Chem. Soc. Jpn.*, 2002, **75**, 1977–1982.
7. K. Yano and Y. Fukushima, *J. Mater. Chem.*, 2003, **13**, 2577–2581.
8. K. Yano and Y. Fukushima, *J. Mater. Chem.*, 2004, **14**, 1579–1584.
9. Y. Yamada and K. Yano, *Micro. Meso. Mater.*, 2006, **93**, 190–198.
10. T. Nakamura, M. Mizutani, H. Nozaki, N. Suzuki and K. Yano, *J. Phys. Chem. C.*, 2007, **111**, 1093–1100.
11. M. Mizutani, Y. Yamada, T. Nakamura and K. Yano, *Chem. Mater.*, 2008, **20**, 4777–4782.
12. K. Yano, M. B. Katz, X. Pan and N. Tatsuda, *J. Colloid Interface Sci.*, 2014, **418**, 61–65.
13. C. Urata, Y. Aoyama, A. Tonegawa, Y. Yamauchi and K. Kuroda, *Chem. Commun.*, 2009, **34**, 5094–5096.

14. Z.-A. Qiao, L.Zhang, M. Guo, Y. Liu and Q. Huo, *Chem. Mater.*, 2009, **21**, 3823–3829.
15. H. Yamada, C. Urata, Y. Aoyama, S.Osada, Y. Yamauchi and K. Kuroda, *Chem. Mater.*, 2012, **24**, 1462–1471.
16. K. Kuroda, A. Shimojima, K. Kawahara, R. Watabayashi, Y. Yamura, Y. Asakura and M. Kitahara , *Chem. Mater.*, 2014, **26**, 211–220.
17. R. I. Nooney, D. Thirunavukkarasu, Y. Chen, R. Josephs and A. E. Ostafin, *Chem. Mater.*, 2002, **12**, 4721–4728.
18. K. Suzuki, K. Ikari and H. Imai, *J. Am. Chem. Soc.*, 2004, **126**, 462–463.
19. K. Ikari, K. Suzuki and H. Imai, *Langmuir*, 2004, **20**, 11504–11508.
20. K. Ikari, K. Suzuki and H. Imai, *Langmuir*, 2006, **22**, 802–806.
21. K. Zhang, L. L. Xu, J.G. Jiang, N. Calin, K. F. Lam, S. J. Zhang, H. H. Wu, G. D. Wu, B. Albela, L. Bonneviot and P. Wu, *J. Am. Chem. Soc.*, 2013, **135**, 2427–2430.

Chapter 3

Morphology Control of Microporous Silica Particles Obtained by Gradual Injection of Reactants

3.1 Introduction

Micro- and mesoporous silica particles are widely used as catalysts and carriers for drug delivery systems (DDS), because of their unique and characteristics pores [1–14]. Among them, those ca. 100 nm in diameter are expected to be useful for applications in DDS and transparent media such as low-refractive index materials, thermal insulation films, and low dielectric materials [6–14]. However, it has been difficult to synthesize monodisperse porous silica particles of 100 nm in diameter on an industrial scale, because the synthesis should take place in highly diluted solutions [10, 15–30]. I have reported in Chapter 2 the large-scale synthesis of monodisperse microporous silica particles of 100 nm in diameter [31], based on the modified Stöber method [32]. This method involves the gradual injection of a silicon alkoxide such as tetramethoxy orthosilicate (TMOS) and a template molecule into the reaction system. The injected TMOS was consumed instantly by the sol-gel reaction. As a result, this system ensures a dilute silicon alkoxide concentration throughout the reaction process, which suppresses the aggregation of the particles. Total amount of the TMOS injected into the system can eventually become large, which is sufficient for an industrial-scale synthesis. In addition, it is possible to obtain monodispersed particles with the present approach. This can be explained by that the concentration of the system is kept constant by the controlled injection of TMOS, which is low enough for the synthesis of monodispersed silica particles via Stöber approach [31]. Thus, the diameter of silica particles saturates at a certain value which depends on the chemical composition and injection kinetics of the procedure. I synthesized monodisperse microporous silica with specific surface area (SSA) of 100 m²/g and diameter of 100 nm in high yield [31]. The applications of microporous silica particles will be accelerated if such particles can be obtained in various morphologies [5–14, 33, 34]. To apply microporous silica in low-refractive index materials and catalysts, the particle diameter and porosity must be controlled without losing yield.

In the current study, I investigate the relationship between the synthetic parameters and morphologies of the resulting silica particles for the system containing n-dodecylamine (DDA) as a template. The influence of injection kinetics and amount of DDA and catalyst on the particle morphology is investigated.

3.2. Experimental

3.2.1 Materials

Methanol (Kanto Chemical Co. Inc., Japan), TMOS (Shin-Etsu, Japan), DDA (TCI, Japan) and 28 % aqueous ammonia (NH₃, Wako Inc., Japan) were used as received. The molar ratio of the reagents in the reaction solution at the end of the injection was TMOS/DDA/NH₃/H₂O = 0.05–0.5/0.1–0.3/0.5–1/2.7–9.9.

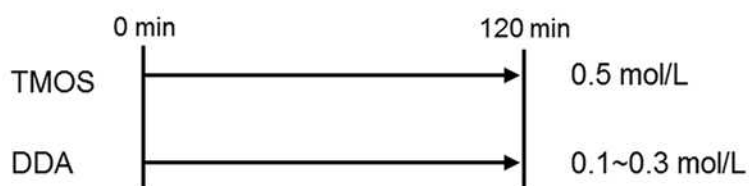
3.2.2 Synthesis

In the case of samples 1–3, two kinds of mixed solution such as NH₃/H₂O/methanol and TMOS/DDA/methanol were prepared. In a typical synthesis procedure, methanol (852.8 g), distilled water (245.2 g) and 28 % aqueous solution of NH₃ (109.6 g) were mixed in a 2 L four-neck flask at 20 °C. Methanol (180.4 g), DDA (37.1 g) and TMOS (137.2 g) were mixed in polyethylene (PE) container, which were then injected into the flask with a tube pump for 120 min under vigorous stirring. The reaction solution was stirred for another 1 h. The resulting precipitates were collected by centrifugation and dried at 120 °C in air for 2 h, and calcined in air at 600 °C for 6 h to remove DDA. (yield: 48.9 g)

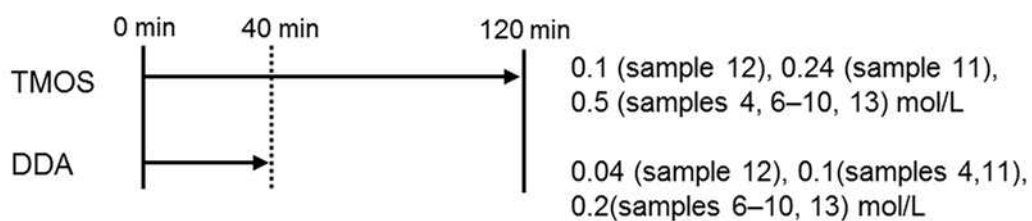
The samples 4–13 were synthesized to see the effect of injection kinetics, where additional TMOS/methanol solution was successively injected after TMOS/DDA/methanol solution. By adjusting respectively the TMOS and DDA concentration of each solution, the injection time of the respective reagents can be controlled (Fig. 3–1). The injection time of DDA for samples 4 and 6–13 were 40 min and for sample 5 was 20 min, while the injection time of TMOS was kept 120 min. The total amount of DDA for samples 4 and 5 was equal to that for sample 1. The amount of DDA for samples 6–13 was twice that for sample 1. Details are summarized in Fig. 3–1 and Table 3–1.

In the case of sample 4, methanol (852.8 g), distilled water (245.2 g), and 28 % aqueous solution of NH₃ (109.6 g) were mixed in a 2 L four-neck flask at 20 °C. The first injection solution containing methanol (60.1 g), DDA (37.1 g) and TMOS (45.7 g) were mixed in PE container, which was injected into the first flask with a tube pump for 40min under vigorous stirring. Subsequently, the second injection solution of methanol (120.4 g) and TMOS

(a) Standard injecting condition (Samples 1–3)



(b) Injection time of DDA was reduced to 40 min (Samples 4 and 6–13)



(c) Injection time of DDA was reduced to 20 min (Sample 5)



Fig. 3–1 Variation of injection time of reactants for (a) samples 1–3, (b) samples 4 and 6–13 and (c) samples 5. The concentration of TMOS and DDA in the resultant solutions are shown on the right.

(91.5 g) in another PE container was injected into the first flask with a tube pump for another 80 min under vigorous stirring. The resultant solution was stirred for 1 h after injection. The resulting precipitates were collected by centrifugation and dried at 120 °C in air for 2 h, and calcined in air at 600 °C for 6 h to remove DDA. (yield: 60.32 g.)

3.2.3 Characterization

Scanning electron microscope (SEM) images were obtained using a JSM-7500TFE microscope (JEOL Ltd., Japan), at an accelerating voltage of 0.5 kV. Transmission electron microscope (TEM) images were obtained using a JEM-2200FS microscope (JEOL Ltd.), at an accelerating voltage of 200 kV. SSA values were determined by the Brunauer Emmett Teller (BET) method, using a SA-6200 instrument (Horiba, Japan). N₂ adsorption-desorption isotherms were obtained at 77 K using a BELSORP-max instrument (BEL Japan Inc., Japan). Samples were pretreated at 373 K for 5 h and then at 473 K for 5 h in a vacuum deaeration. Pore size distributions were calculated using MP methods.

3.3. Results and Discussion

The compositions of the resultant solutions and physical parameters of each sample are listed in Table 3–1. The effects of the amount and injection time of DDA on SSA were investigated with samples 1–3 and samples 4–6, respectively. The relationship between the hydrolysis kinetics and particle diameters was investigated, by changing the amount of catalysts such as ammonia and water for samples 7–10. Aggregation was suppressed by optimizing the TMOS concentration in samples 11–13.

Table 3–1. Compositions of the resultant solutions (after completion of the injection) and obtained physical parameters of the synthesized silica particles.

Sample	DDA/ TMOS	[TMOS]	[H ₂ O]	[NH ₃]	Injection time of MeOH/TMOS/DDA solution	Injection time of MeOH/TMOS solution	Particle diameter	SSA (adsorption)
1	1/5	0.5	9.5	1	120	-	130	130
2	2/5	0.5	9.3	1	120	-	130	320
3	3/5	0.5	9.1	1	120	-	130	490
4	1/5	0.5	9.5	1	40	80	100–150	220
5	1/5	0.5	9.5	1	20	100	100–200	140
6	2/5	0.5	9.3	1	40	80	N.A. (Aggregated)	1030
7	2/5	0.5	9.5	0.5	40	80	300–400	400
8	2/5	0.5	4.3	0.7	40	80	40	220
9	2/5	0.5	3.0	0.7	40	80	30	170
10	2/5	0.5	2.7	0.7	40	80	20	290
11	2/5	0.24	9.6	1	40	80	150–250	720
12	2/5	0.1	9.8	1	40	80	400	1070
13	2/5	0.05	9.9	1	40	80	250	620

3.3.1 Effect of DDA Amount (Samples 1–3)

The microporous silica particles synthesized in Chapter 2 were 130 nm of diameter and 130 m²/g of SSA [sample 1, 31]. From the view point of the property control, it is important to synthesize the silica particles with variety of SSA and diameter. I synthesized silica particles using three different amounts of DDA to see an effect of the amount of a surfactant on the porosity. The SSA values and particle diameter distributions of the resultant silica particles were examined, and the results are summarized in Table 3–1.

SEM images of silica particles of samples 1, 2 and 3 are shown in Fig. 3–2. A TEM image of silica particles of sample 3 is shown in Fig. 3–3. The SSA values and pore volume increased with the increase of the DDA amount, while the particle size and pore size distribution remained constant (Fig. 3–4). In other words, the number of pores increased without altering the pore diameters. Those data shows that the SSA can be tuned from 100 to 500 m²/g, without changing the particle size. Microporous silica particles of narrow diameter distribution were obtained irrespective of DDA amount, but some aggregation, where two or more silica particles were merged each other, was observed for samples synthesized using larger amounts of DDA (Fig. 3–3). In general, the aggregation of silica particles is suppressed in basic media by the electrostatic repulsion of the deprotonated silanol groups on the surface. However, DDA can get adsorbed on the silica surface through hydrogen bonding between Si–OH and NH₂-groups, which makes the outside of the particle covered by the nonionic alkyl chains of DDA. Thus, the electrostatic repulsion was suppressed by the nonionic alkyl chains on particle surface, resulting in some aggregation.

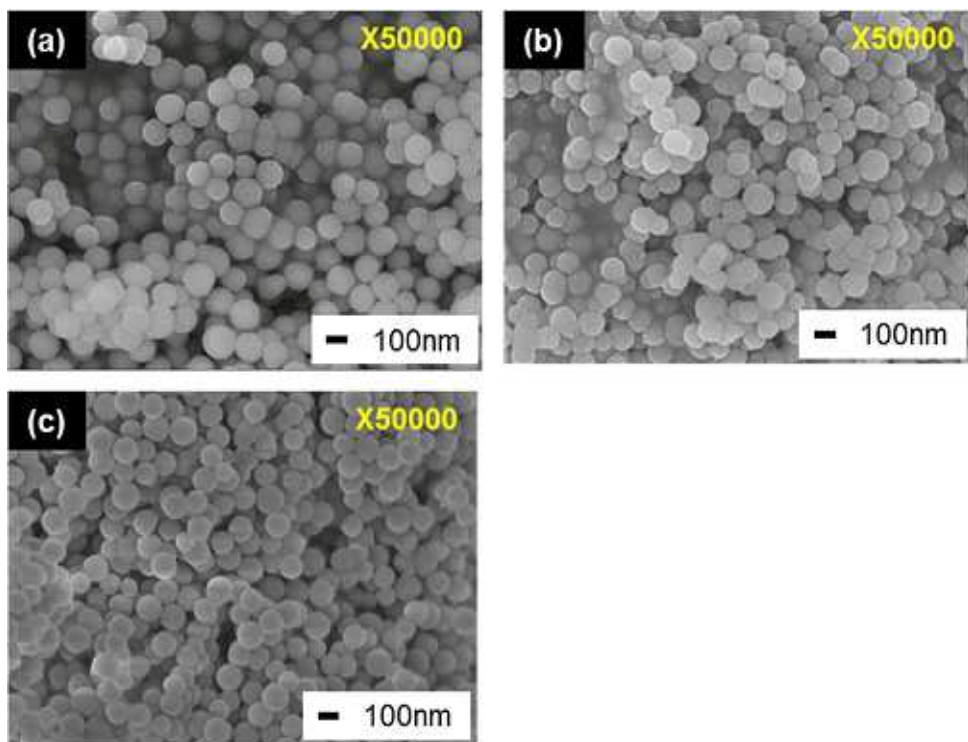


Fig. 3–2 SEM images of porous silica particles of (a) sample 1, (b) sample 2 and (c) sample 3.

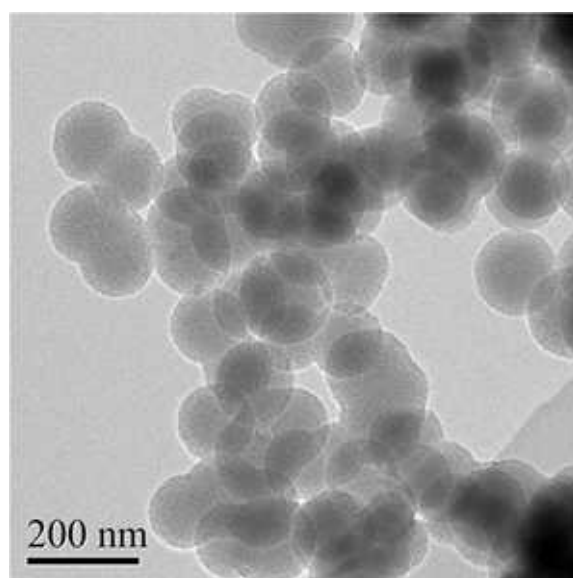


Fig. 3-3 TEM image of porous silica particles of sample 3.

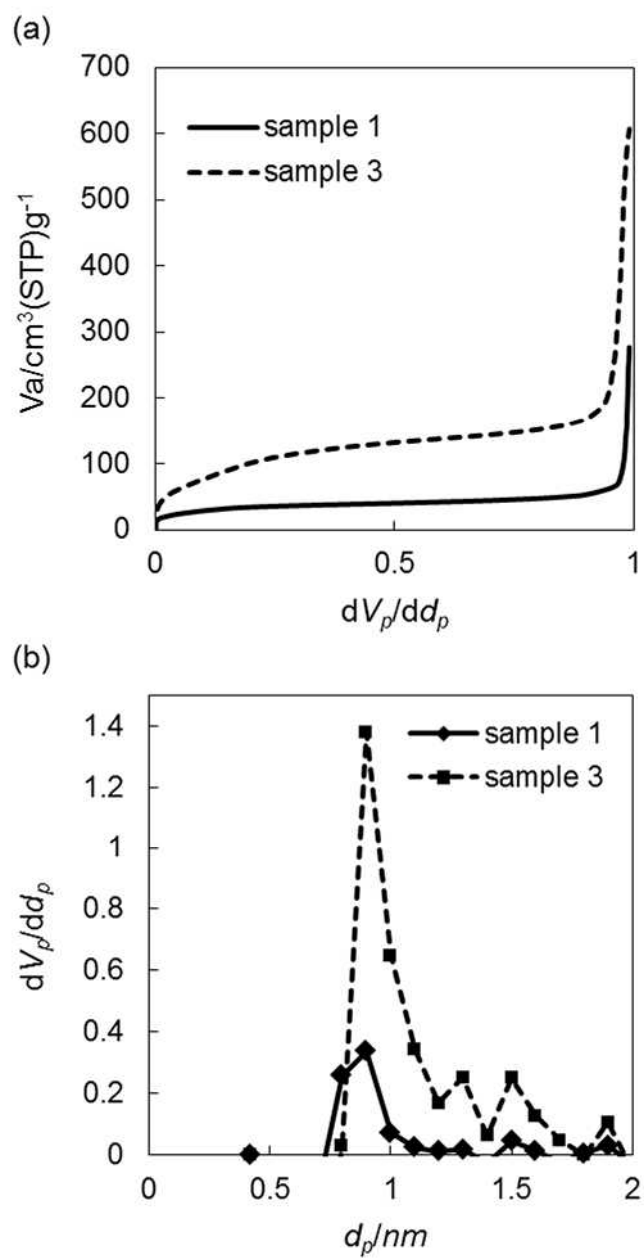


Fig. 3-4 (a) Nitrogen adsorption isotherms and (b) pore size distribution curves from MP method of obtained silica of samples 1 and 3.

3.3.2 Effect of DDA Injection Time (Samples 4–6)

An advantage of the present protocol is that the kinetics of the chemical reactions can be controlled by successive (or parallel) injection of different solutions. As is explained in the experimental section, the successive injection of the solutions with different compositions was carried out to examine the effect of injection kinetic on the resultant morphologies of the porous silica nano-particles. For example, in the case of sample 4, TMOS/DDA/methanol mixture was injected for the first 40 min, and then the TMOS/methanol solution was injected for another 80 min. The total amounts of DDA and TMOS were identical to sample 1. That is to say, in comparison with sample 1 the injection time of DDA for sample 4 was decreased from 120 min to 40 min, while that of TMOS was kept the same 120 min. This operation enables us to control the injection time of each reactant independently.

The effect of DDA injection time on the particle morphology was examined. The injection time of DDA for samples 4–6, was decreased compared with that for sample 1 (Fig. 3–1). The amount of DDA incorporated in the silica matrix was expected to be increased by enriching DDA concentration at the initial stages of reaction process. The injection times of DDA for samples 4 and 5 were 40 and 20 min, respectively, while the injection time of TMOS was maintained at 120 min. The total amount of DDA was the same for samples 1, 4 and 5. The amount of DDA in sample 6 was increased, which was twice that in sample 4. These details are summarized in Fig. 3–1 and Table 3–1.

TEM images of silica particles of samples 4, 5, and 6 are shown in Fig. 3–5. The particle sizes and the distribution of the sizes for samples 4–6 were larger than those of sample 1. Aggregated particles were found in samples 4–6. Comparing samples 1 (Fig. 3–2 (a)) and 4–5, it seems to be more difficult to obtain the monodispersed particles for shorter DDA injection times. The particle aggregation, which two or more silica particles were connected, was occurred in samples 4 and 5. The SSA was independent of DDA injection time (Table 3–1). Significant aggregation occurred for samples in which more DDA had been injected earlier in the reaction. This is because electrostatic repulsion between the particles is suppressed by an adsorption of DDA on the silica particles forming the nonionic surfaces. Accordingly, the particle size distribution became difficult to control.

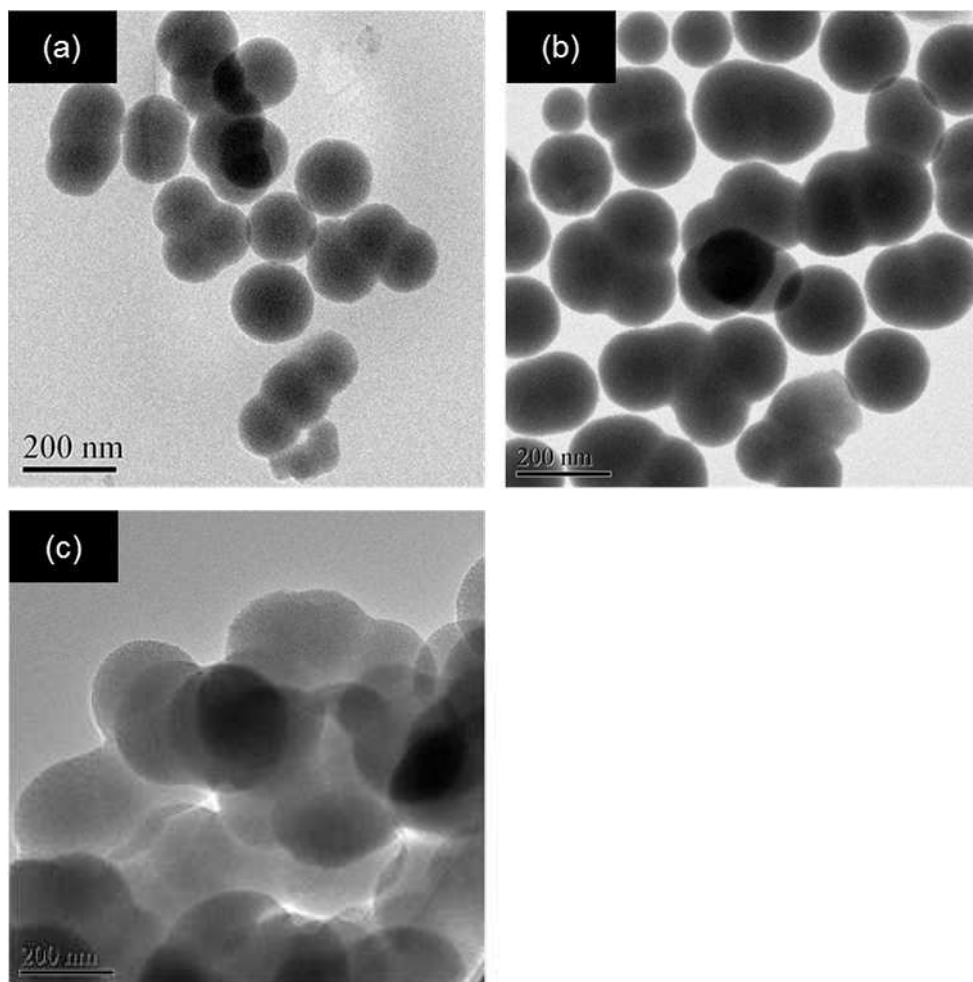


Fig. 3-5 TEM images of porous silica particles of (a) sample 4, (b) sample 5 and (c) sample 6.

Significant aggregation was also observed for sample 6. It was considered that abnormal grain growth occurred by the interaction between growing silica particles, also due to excess DDA. Sample 6 was prepared under the same synthetic condition as sample 5 for the first 20 min of DDA injection, but DDA injection was then continued for another 20 min. Thus, the total DDA content was twice that of sample 5. The SSA of sample 6, which was synthesized with shorter DDA injection time than sample 2 using the same amount of DDA, was more than three times that of sample 2. This means that more DDA is incorporated into silica matrix for sample 6. As same as samples 4 and 5, excess DDA on the surface of the silica particles reduces the electrostatic repulsion, leading to a loss of mono dispersibility. The shorter DDA injection time yielded silica particles with a larger SSA, but their aggregation occurred at the same time. I have reported in Chapter 2 that although SSA could be increased by injection of TMOS into the basic aqueous solution containing DDA, controlling the particle size became more difficult [31]. This finding is in agreement with the present results. The extra DDA adsorbed on the silica particles, and electrostatic repulsion was suppressed by nonionic alkyl chains on the particle surfaces. Thus, the shorter DDA injection time resulted in aggregation. Short injection time yielded microporous silica particles with larger SSA, but their size distribution could not be easily controlled.

3.3.3 Effect of Amount of Catalyst and Water (Samples 7–10)

The SSA of sample 6 was exceeding $1000 \text{ m}^2/\text{g}$, which was the largest among the samples synthesized here, but significant aggregation was taken place. Based on this result, a variety of the synthetic conditions were examined to elucidate the relationship between preparation conditions and physical properties of the particle. Considering that the hydrolysis and polycondensation kinetics have influence on the morphology of the resulting particles [10, 26–29, 32, 35, 36], the effects of concentrations of the ammonia or water on particle morphology were evaluated.

Sample 7 was prepared using half the amount of ammonia used in sample 6, its particle size was larger as shown in Fig. 3–6 (a). The particle size typically increases in less basic conditions because the electric repulsion on the surface of silica particles becomes weak [36]. Therefore, the particle size of sample 7 was larger than that of sample 6.

For systems containing less water (samples 8–10 shown in Fig. 3–6 (b)–(d)), the particle diameter and SSA tended to be smaller than those of sample 6. Under these conditions, the silanol group content produced by the hydrolysis of TMOS was lower. This suppressed the nucleation reaction, which usually increased the particle diameter. But in the present cases, the diameter of silica particle was smaller under the condition involved less water. It was deduced that the growth reaction was suppressed by increasing electric repulsion of silica surface because of the better solubility of DDA in the reaction solution and that reducing the interaction of DDA with silica oligomers. The SSA also decreased because DDA was not sufficiently incorporated into silica, owing to the fewer surface silanol groups interacting with DDA. The SSA of sample 10 was larger than that of sample 9, because of the textual pores between primary particles. These results indicated that the most important parameters for controlling particle size were the amounts of water and catalyst.

3.3.4 Effect of TMOS Concentration (Samples 11–13)

The TMOS concentration of the reaction solution was lowered in attempt to avoid particle aggregation. Fig. 3–7 shows TEM images of silica particles from samples 11, 12, and 13. There was no obvious relationship between particle diameter and SSA with TMOS concentration. Controlling the silica particle morphology was very difficult in these cases. The resulting particles were not monodisperse in the presence of extra DDA, for the same reason as for sample 6. The dilution of TMOS did little to regulate particle formation, because the TMOS concentration was already diluted enough.

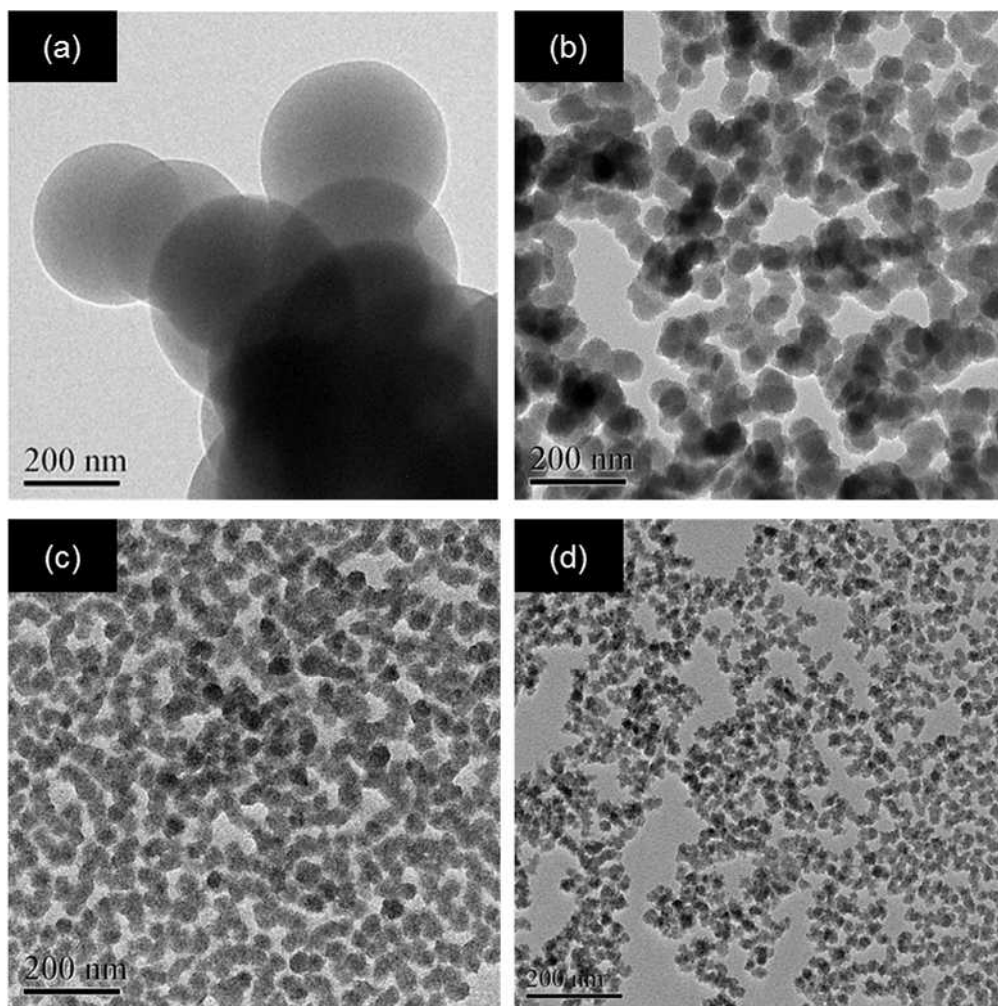


Fig. 3-6 TEM images of porous silica particles of (a) sample 7, (b) sample 8, (c) sample 9 and (d) sample 10.

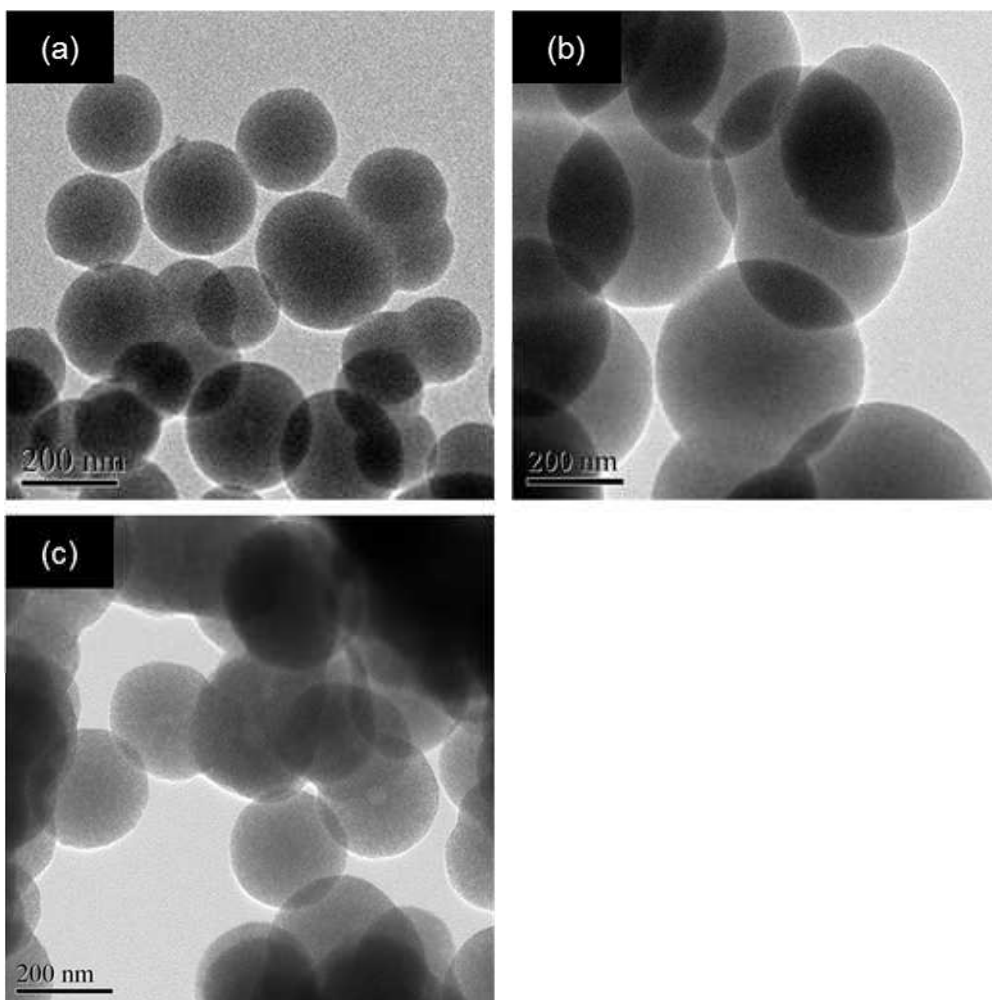


Fig. 3-7 TEM images of porous silica particles of (a) sample 11, (b) sample 12 and (c) sample 13.

The relationship between the conditions of reaction and silica particle size and SSA are shown in Fig. 3–8. It was found that SSA of silica nano-particles depended on DDA amount and injection time, while the particle diameter did not depend on the DDA/TMOS ratio. The dispersibility of the particles was difficult to control by the experimental conditions mentioned above. Monodisperse microporous silica particles of 100–150 nm in diameter could only be synthesized under the conditions applied for samples 1–4.

3.4 Conclusion

Microporous silica particles of 20–200 nm in particle diameter and 100–1000 m²/g in SSA were synthesized by the gradual injection of reagents into the reaction system. Increasing the amount of DDA and shortening the DDA injection time yielded particles with larger diameters and SSA values, which also caused aggregation. Changing only the DDA amount allowed the SSA to be tuned from 100 to 500 m²/g without changing the particle size. The most important parameters for controlling the particle size were the amounts of water and ammonia. This method is effective for synthesizing microporous silica with various morphologies.

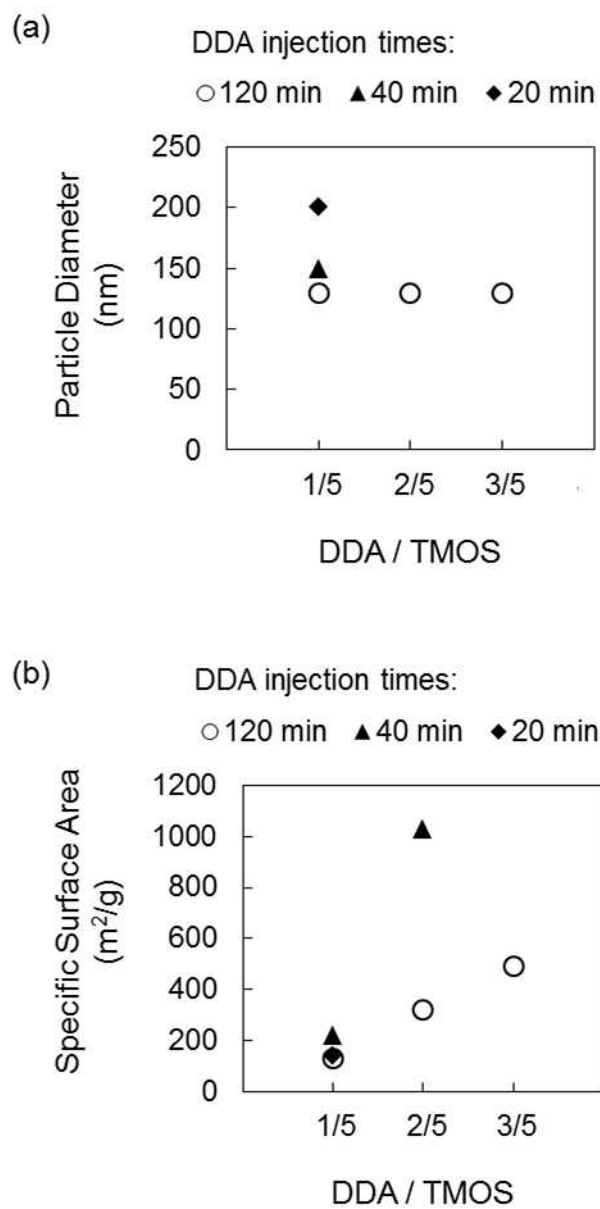


Fig. 3-8 Relationship between the DDA/TMOS ratio and (a) particle diameter (and) b SSA for different DDA injection times (20, 40, and 120 min).

References

1. T. Maschmeyer, F. Rey, G. Sankar and J. M. Thomas, *Nature*, 1995, **378**, 159–162.
2. J. P. K. Reynhardt, Y. Yang, A. Sayari and H. Alper, *Chem. Mater.*, 2004, **16**, 4096–4102.
3. N. Mizoshita, T. Tani and S. Inagaki, *Chem. Soc. Rev.*, 2011, **40**, 789–800.
4. Y. Belmoujahid, M. Bonne, Y. Scudeller, D. Schleich, Y. Grohens and B. Lebeau, *Microporous and Mesoporous Materials*, 2015, **201**, 124–133.
5. S. Yoda, M. Ohara, Y. Takebayashi, K. Sue, Y. Hakuta, T. Furuya, M. Yamadab and K. Otake, *J. Mater. Chem. A*, 2013, **1**, 9620–9623.
6. F. Lu, S. -H. Wu, Y. Hung and C. -Y. Mou, *Small*, 2009, **5** (12), 1408–1413.
7. X. Du and J. He, *Nanoscale*, 2011, **3**, 3984–4002.
8. C. Barbé, J. Bartlett, L. Kong, K. Finnie, H. Q. Lin, M. Larkin, S. Calleja, A. Bush and G. Calleja, *Adv. Mater.*, 2004, **16**, 1959–1966.
9. S. Kwon, R. K. Singh, R. A. Perez, E. A. A. Neel, H. -W. Kim and W. Chrzanowski, *J. Tissue Eng.*, 2013, **4**, 1–18.
10. H. Yamada, C. Urata, Y. Aoyama, S. Osada, Y. Yamauchi and K. Kuroda, *Chem. Mater.*, 2012, **24**, 1462–1471.
11. Y. -S. Lin, K. R. Hurley and C. L. Haynes, *J. Phys. Chem. Lett.*, 2012, **3**, 364–374.
12. C. Urata, H. Yamada, R. Wakabayashi, Y. Aoyama, S. Hirose, S. Arai, S. Takeoka, Y. Yamauchi and K. Kuroda, *J. Am. Chem. Soc.*, 2011, **133**, 8102–8105.
13. J. Kobler and T. Bein, *ACS Nano*, 2008, **11**, 2324–2330.
14. M. Nakamura, M. Shono and K. Ishimura, *Anal. Chem.*, 2007, **79**, 6507–6514.
15. R. I. Nooney, D. Thirunavukkarasu, Y. Chen, R. Josephs and A. E. Ostafin, *Chem. Mater.*, 2002, **12**, 4721–4728.
16. K. Ikari, K. Suzuki and H. Imai, *Langmuir*, 2004, **20**, 11504–11508.
17. K. Suzuki, K. Ikari and H. Imai, *J. Am. Chem. Soc.*, 2004, **126**, 462–463.
18. K. Ikari, K. Suzuki and H. Imai, *Langmuir*, 2006, **22**, 802–806.
19. K. Yano, N. Suzuki, Y. Akimoto and Y. Fukushima, *Bull. Chem. Soc. Jpn.*, 2002, **75**, 1977–1982.
20. K. Yano and Y. Fukushima, *J. Mater. Chem.*, 2003, **13**, 2577–2581.

21. K. Yano and Y. Fukushima, *J. Mater. Chem.*, 2004, **14**, 1579–1584.
22. Y. Yamada and K. Yano, *Micro. Meso. Mater.*, 2006, **93**, 190–198.
23. M. Mizutani, Y. Yamada, T. Nakamura and K. Yano, *Chem. Mater.*, 2008, **20**, 4777–4782.
24. K. Yano, M. B. Katz, X. Pan and N. Tatsuda, *J. Colloid Interface Sci.*, 2014, **418**, 61–65.
25. C. Urata, Y. Aoyama, A. Tonegawa, Y. Yamauchi and K. Kuroda, *Chem. Commun.*, 2009, **34**, 5094–5096.
26. H. Yamada, C. Urata, H. Ujiie, Y. Yamauchi and K. Kuroda, *Nanoscale*, 2013, **5**, 6145–6153.
27. K. Kuroda, A. Shimojima, K. Kawahara, R. Watabayashi, Y. Yamura, Y. Asakura and M. Kitahara, *Chem. Mater.*, 2014, **26**, 211–220.
28. K. Möller, J. Kobler and T. Bein, *Adv. Funct. Mater.*, 2007, **17**, 605–612.
29. Z.-A. Qiao, L. Zhang, M. Guo, Y. Liu and Q. Huo, *Chem. Mater.*, 2009, **21**, 3823–3829.
30. K. Zhang, L. L. Xu, J.G. Jiang, N. Calin, K. F. Lam, S. J. Zhang, H. H. Wu, G. D. Wu, B. Albel, L. Bonneviot and P. Wu, *J. Am. Chem. Soc.*, 2013, **135**, 2427–2430.
31. T. Shimogaki, H. Tokoro, M. Tabuchi, N. Koike, Y. Yamashina and M. Takahashi, *J. Sol-Gel Sci. Technol.*, 2015, **74**, 109–113.
32. W. Stöber and A. Fink, *J. Colloid Interface Sci.*, 1968, **26**, 62–69.
33. H. Watanabe, K. Fujikata, Y. Oaki and H. Imai, *Chem. Commun.*, 2013, **49**, 8477–8479.
34. J. E. Lofgreen and G. A. Ozin, *Chem. Soc. Rev.*, 2014, **43**, 911–933.
35. S. -H. Wu, C. -Y. Mou and H. -P. Lin, *Chem. Soc. Rev.*, 2013, **42** (9), 3862–3875.
36. C. J. Brinker and G. W. Scherer, *Sol-Gel Science: The Physics and Chemistry of Sol-Gel Processing*; Academic Press: Boston, 1990.

Chapter 4

Large- Scale Preparation of Morphology- Controlled Microporous Silica Particles via Gradual Injection of Reactants with Different Surfactants

4.1 Introduction

Porous silica particles with diameters of ca. 100 nm can be practically utilized for applications in drug delivery systems and transparent materials [1–14]. However, the industrial-scale synthesis of monodispersed and microporous silica particles with diameters in this range remains difficult. Such silica particles are usually prepared with highly diluted solutions, resulting in inefficient processing [6, 7, 15–31]. Recently, I have reported the industrial-scale synthesis of monodisperse microporous silica particles of ca. 100 nm in diameter [Chapter 2, 32] based on a modified Stöber method [33]. The processing is characterized by a gradual and controlled injection of a silicon alkoxide such as tetramethoxy orthosilicate (TMOS) and a template molecule into the reaction system. The injected TMOS is consumed instantly by the sol-gel reaction; thus, the system remains diluted throughout the preparation process. The total amount of TMOS injected into the system can eventually become sufficient for large-scale fabrication, which enables us to obtain 10 times more silica particles than can be formed using previous synthetic methods. The obtained silica particles show a narrow distribution of particulate diameter. Using n-dodecylamine (DDA) as a template molecule, the monodisperse, microporous silica particles with diameters ranging from 20 to 200 nm and specific surface area (SSA) from 100 to 1000 m²/g can be obtained by adjusting the synthetic parameters [Chapter 3, 34].

In the present Chapter, to achieve the synthesis of microporous silica particles with a broad range of morphologies via gradual injection of reactants, I investigated the effect of template molecules on the porosity and morphology of the resultant silica particles. In particular, an attempt was made to achieve the preparation of silica nano-particles with a larger SSA while maintaining the particle diameter at approximately 100 nm. Ammonium salts, which are strongly basic, and primary and secondary amines with different chain lengths were used as template molecules.

4.2 Experimental

4.2.1 Materials

Methanol (Kanto Chemical Co., Inc., Japan), TMOS (Shin-Etsu, Japan), 28 % aqueous ammonia (NH₃, Wako Inc., Japan), and DDA, dodecyltrimethylammoniumbromide (DTAB), benzylamine, octylamine, decylamine (DA), tetradecylamine, hexadecylamine, stearylamine, oleylamine, and N,N-dimethyldodecylamine (TCI, Japan), were used as received. The molar ratio of the reagents in the reaction solution at the end of the injection was TMOS/template molecule/NH₃/H₂O = 0.5/0.1–0.5/1.0/9.5.

4.2.2 Synthesis

In a typical synthesis procedure, two kinds of mixed solution, such as NH₃/H₂O/methanol (reaction solution) and TMOS/template molecule/methanol (injection solution), were prepared. In sample 1, for example, methanol (852.8 g), distilled water (245.2 g), and a 28 % aqueous solution of NH₃ (109.6 g) were mixed in a 2 L four-neck flask at 20 °C. Methanol (180.4 g), DDA (37.1 g), and TMOS (137.2 g) were mixed in a polyethylene container and then injected into the flask with a tube pump for 120 min under vigorous stirring. The reaction solution was stirred for another 1 h. The resulting precipitates were collected by centrifugation, dried at 120 °C in air for 2 h, and calcined in air at 600 °C for 6 h to remove DDA (yield: 48.9 g).

In the case of sample 3, DTAB as a template molecule was added to the ‘reaction solution’ and not the ‘injection solution’. Specifically, the two kinds of mixed solution were template molecule/NH₃/H₂O/methanol (reaction solution) and TMOS/methanol (injection solution).

4.2.3 Characterization

Scanning electron microscope (SEM) images were obtained using a JSM-7500TFE microscope (JEOL Ltd., Japan) at an accelerating voltage of 0.5 kV. Transmission electron microscope (TEM) images were obtained using a JEM-2200FS microscope (JEOL Ltd.) at an accelerating voltage of 200 kV. SSA values were determined by the Brunauer–Emmett–Teller

method using an SA-6200 instrument (Horiba, Japan). N₂ adsorption-desorption isotherms were obtained at 77 K using a BELSORP-max instrument (BEL Japan Inc., Japan). Samples were pretreated at 373 K for 5 h and then at 473 K for 5 h in a vacuum deaeration. Pore size distributions were calculated using MP methods. Dynamic light scattering (DLS) measurements were recorded using an ELSZ-1000 instrument (Otsuka Electronics, Japan).

4.3 Results and Discussion

The type of template molecule, composition, and some physical parameters of the resultant silica particles are summarized in Table 4–1. An example of porosity distributions are shown in Fig. 4–1. Sample 1 was used as the standard condition in the present work. Samples 2 and 3 were prepared to determine the efficacy of ammonium salt as a template molecule on the morphology of silica particles. Samples 4–11 were fabricated to test the influence of alkyl chain length on the SSA of silica particles using primary and tertiary amines with different alkyl chain lengths. Samples 12 and 13 were synthesized to achieve silica particles of 100 nm in diameter with higher SSA than that of sample 1 by adjusting the amount of amines.

Table 4–1 Type of template molecule (TM), octanol/water partition coefficient ($\log P_{ow}$) of TM, TM/TMOS ratio, and morphology, diameter, SSA and pore alignment of the resultant silica.

Sample	Template molecules (TM)	Log P_{ow} of TM	TM / TMOS (mol/mol)	Morphology	Particle diameter (nm)	SSA (adsorption) (m^2/g)	Pore alignment
1	DDA	4.76	1 / 5	particle	130	130	disorder
2	Dodecyltrimethyl -ammoniumbromide		1 / 5	particle	200 ~300	430	disorder
3*	Dodecyltrimethyl -ammoniumbromide		1 / 5	particle	>500	660	disorder
4	benzylamine	1.09	1 / 5	particle	100	40	disorder
5	octylamine	3.10	1 / 5	particle	100	40	disorder
6	decylamine	4.12	1 / 5	particle	100	60	disorder
7	tetradecylamine	6.24	1 / 5	particle	150	490	disorder
8	hexadecylamine	7.17	1 / 5	sheet	-	300	disorder
9	stearylamine	8.37	1 / 5	sheet	-	240	disorder
10	oleylamine	7.85	1 / 5	rectangular	-	580	disorder
11	N,N-dimethyl -dodecylamine	5.91	1 / 5	particle	100	40	disorder
12	decylamine	4.12	4 / 5	particle	100	530	disorder
13	decylamine	4.12	5 / 5	particle	100	530	disorder

* Template molecule was in reaction solution.

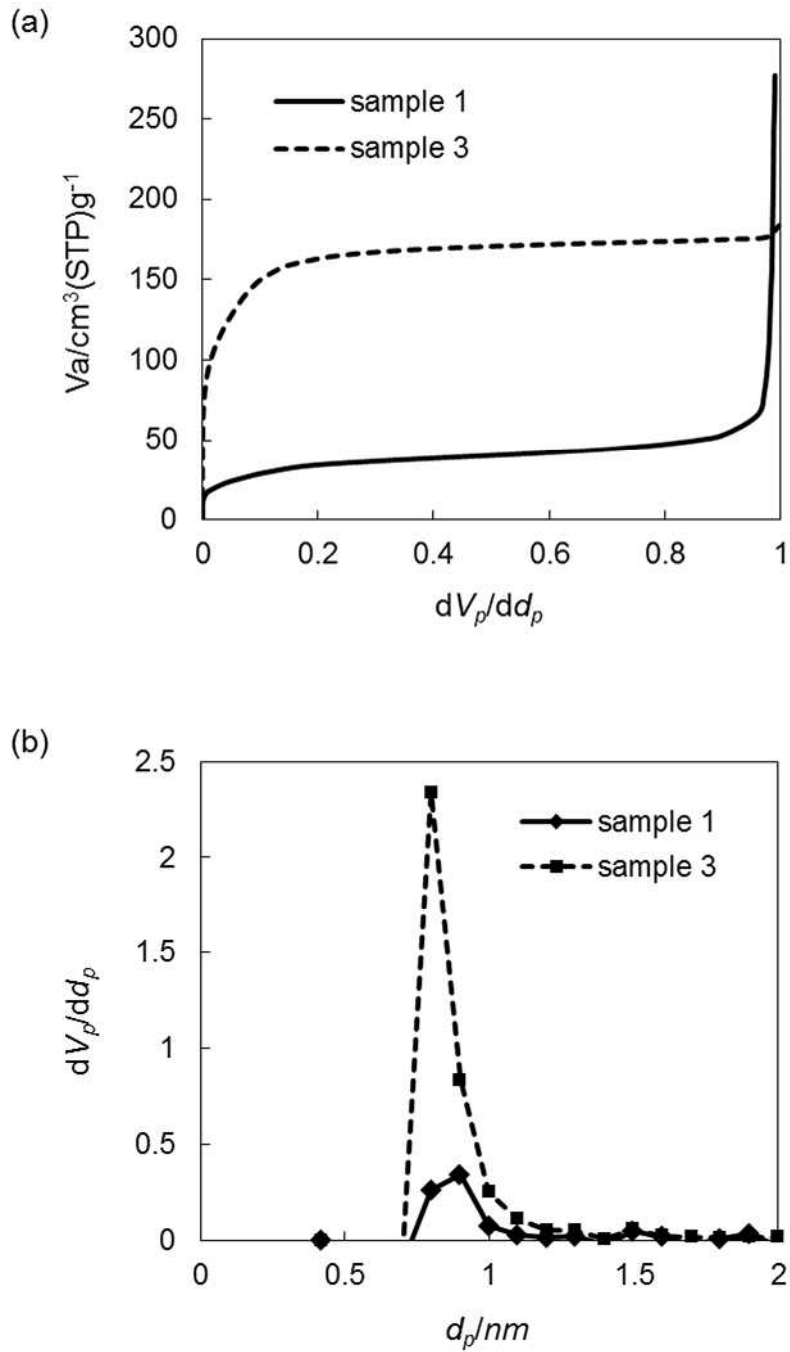


Fig. 4-1 (a) Nitrogen adsorption isotherms and (b) pore size distribution curves from MP method of obtained silica of samples 1 and 3.

4.3.1 Ammonium Salts as Template Molecules

In samples 2 and 3, the efficacy of ammonium salts as template molecules was investigated and compared with sample 1. DTAB, which has the same alkyl chain length of DDA, was used as a template molecule. The injection method of DTAB was different for samples 2 and 3. In sample 2, DTAB was injected with TMOS for 120 min, the same as sample 1. In sample 3, only the TMOS/methanol solution was injected, while DTAB was dissolved in the reaction solution. TEM images of the obtained silica particles are shown in Fig. 4–2.

Even though they had the same alkyl chain length, both the SSA and particle diameter of sample 2 are larger than those of sample 1. Generally, the basicity of the ammonium salt is stronger than that of alkyl amines. As a result, DTAB can strongly interact with silanol groups, and more DTAB can be accommodated in the silica matrix. The particle diameter and distribution are large in sample 2 because the pH of the reaction solution is higher than that of sample 1 because of the introduction of ammonium salt. Hydrolysis and polycondensation reactions are expected to proceed faster than in the case of sample 1, resulting in larger particles and more severe aggregation in sample 2. Furthermore, the aggregation is particularly noticeable in sample 3 because DTAB, which has strong effects on particle morphology, was presented in the reaction solution from the initial stage of the sol-gel reaction. These results show that ammonium salts are effective template molecules for the synthesis of microporous silica particles with high SSA and diameters greater than 200 nm. The pore alignments of these samples were disordered, and the porous size were almost the same (Fig. 4–1).

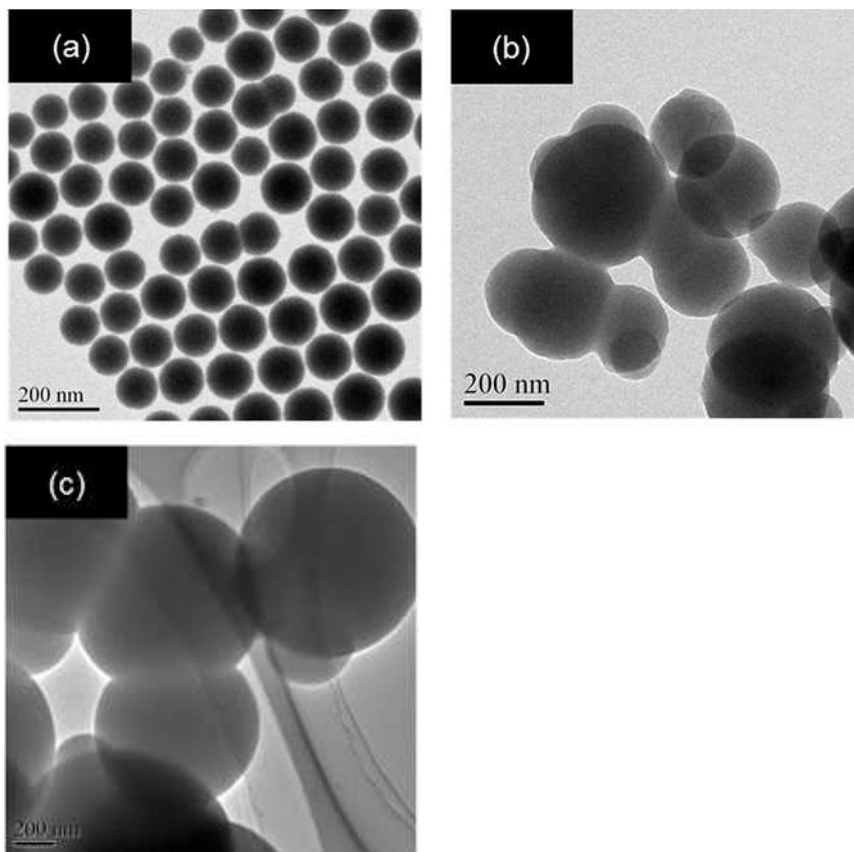


Fig. 4-2 TEM images of porous silica particles: (a) sample 1, (b) sample 2 and (c) sample 3.

4.3.2. Effect of Alkyl Chain Length

The effect of alkyl chain length of alkyl amines on the resultant morphologies is examined with samples 4–11. The SEM images of the resultant silica particles are shown in Fig. 4–3. SSA increases with alkyl chain length, as shown in Table 4–1. The pore alignments of all samples were disordered. In particular, the SSA of the resultant silica particles prepared with alkyl amines bearing an alkyl chain of over 12 carbons exceeded 100 m²/g. Conversely, in the case of alkyl amines with > 16 carbons, the morphology of the obtained porous silica is not particle-like anymore, but rather sheet-like or rectangular. Amines with an octanol/water partition coefficient ($\log P_{ow}$) >7 exhibit lower solubility in the reaction solution. As a result, the amines show a tendency to precipitate from the reaction solution, becoming nucleation sites for the sol-gel reaction. Comparing samples 9 and 10, which have the same alkyl chain length but different $\log P_{ow}$ values, the morphology of sample 10 is particle-like, but that of sample 9 is not. This indicates that the $\log P_{ow}$ value is an important factor for controlling silica morphology. In particular, using amines with good solubility in the reaction solution, such as $\log P_{ow} < 7$, is required to synthesize spherical silica particles. Sample 11, prepared with a tertiary amine as a template molecule, shows spherical shape, but its SSA is only 40 m²/g. It is possible that the interaction between amine and silanol is not large enough to generate pores because of the large steric hindrance of the tertiary amine. These results suggest that the most effective template molecule to obtain monodisperse and spherical microporous silica particles with diameters of approximately 100 nm is a primary amine with a $\log P_{ow} < 7$.

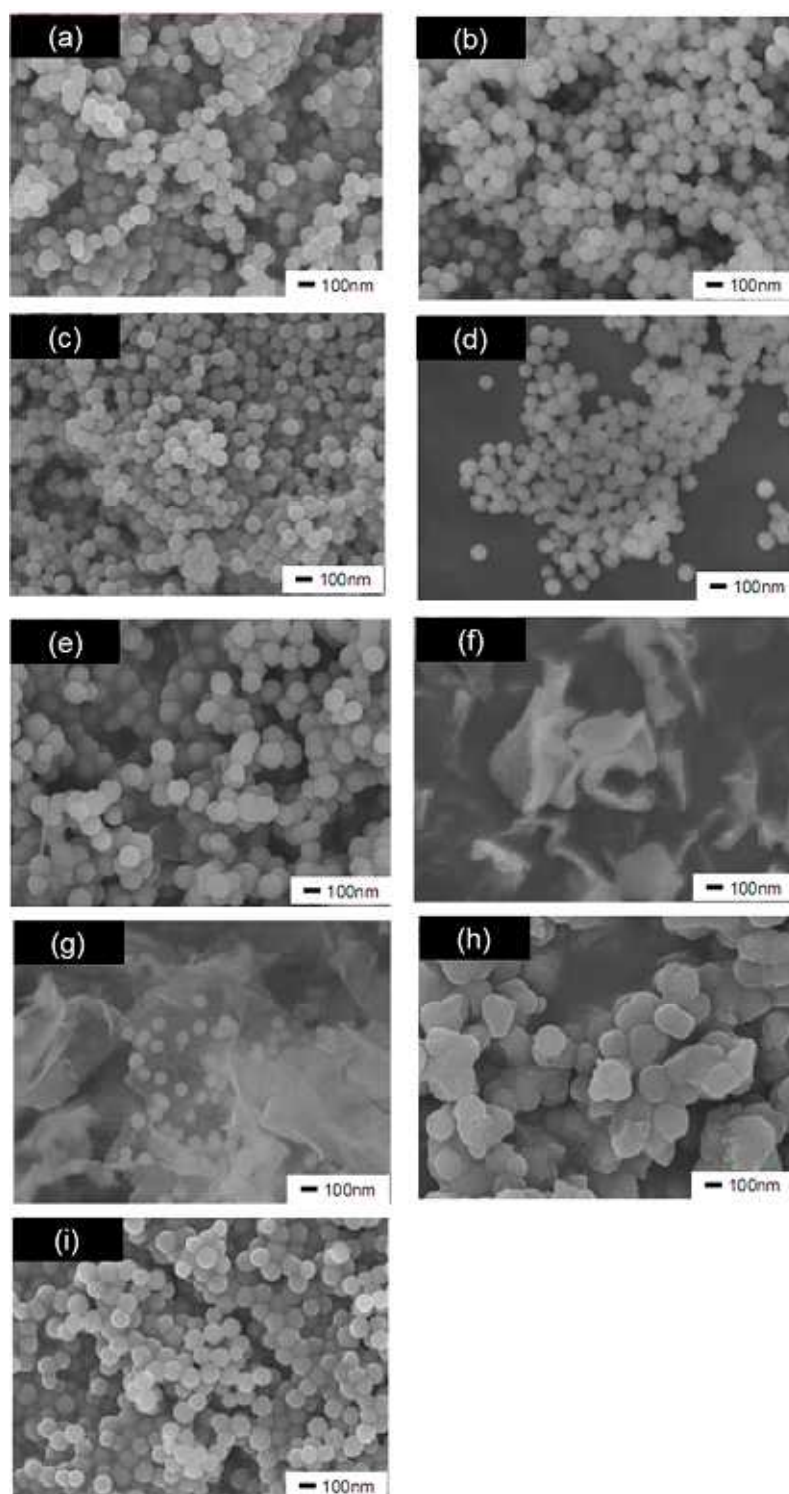


Fig. 4-3 SEM images of porous silica particles: (a) sample 1, (b) sample 4, (c) sample 5, (d) sample 6, (e) sample 7, (f) sample 8, (g) sample 9, (h) sample 10 and (i) sample 11.

4.3.3. Effect of Concentration of Template Amines and Reaction Time

The effect of concentration of template molecules on SSA was also examined. I have reported in Chapter 3 that the aggregation of particles is more frequent with higher concentrations of DDA [34]. Samples 12 and 13 were prepared to obtain monodispersed and microporous silica particles with higher SSA using DA as a template molecule, which exhibits a better solubility in reaction solution than DDA. TEM images of obtained silica particles are shown in Fig. 4-4. Samples 12 and 13 were obtained with 4 and 5 times more DA than that of sample 6. The resultant silica particles of both sample 12 and 13 were 80–100 nm in diameter with good dispersibility and high SSA (530 m²/g).

To observe the particle growth, aliquots of the reaction mixture were collected at regular time intervals during the preparation of sample 12. The SEM images are shown in Fig. 4-5, and particle size distribution vs. reaction time is shown in Fig. 4-6. In Figs. 4-5 and 4-6, it can be observed that the particle diameter gradually increases with increasing reaction time. The particle size distribution is wide after 10 min from injection, and then decreases with reaction time. This can be explained by Ostwald ripening [35], which indicates that the solubility of newly generated small particles in the reaction solution is higher than that of larger silica particles. In this case, the rate-determining process of particle formation is nucleation. Furthermore, the larger particles grew more slowly than smaller particles because smaller particles possess larger SSAs, and therefore more TMOS reaction sites, than larger ones. The particle size distribution narrowed in the later stages of reaction, despite continuous nucleation occurring during TMOS injection.

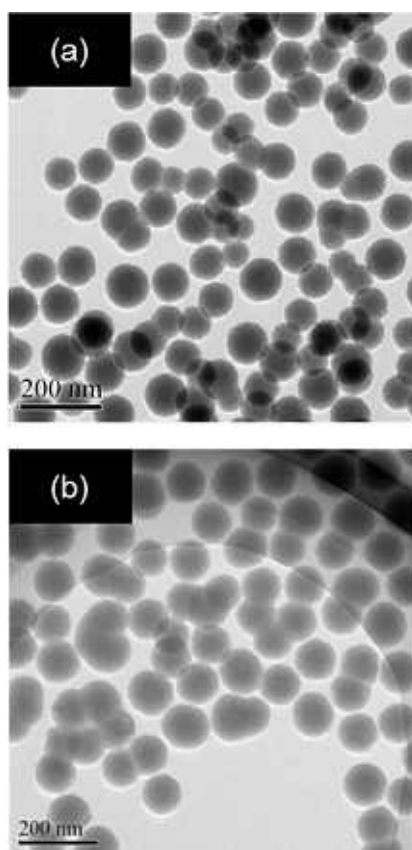


Fig. 4-4 TEM images of porous silica particles: (a) sample 12 and (b) sample 13.

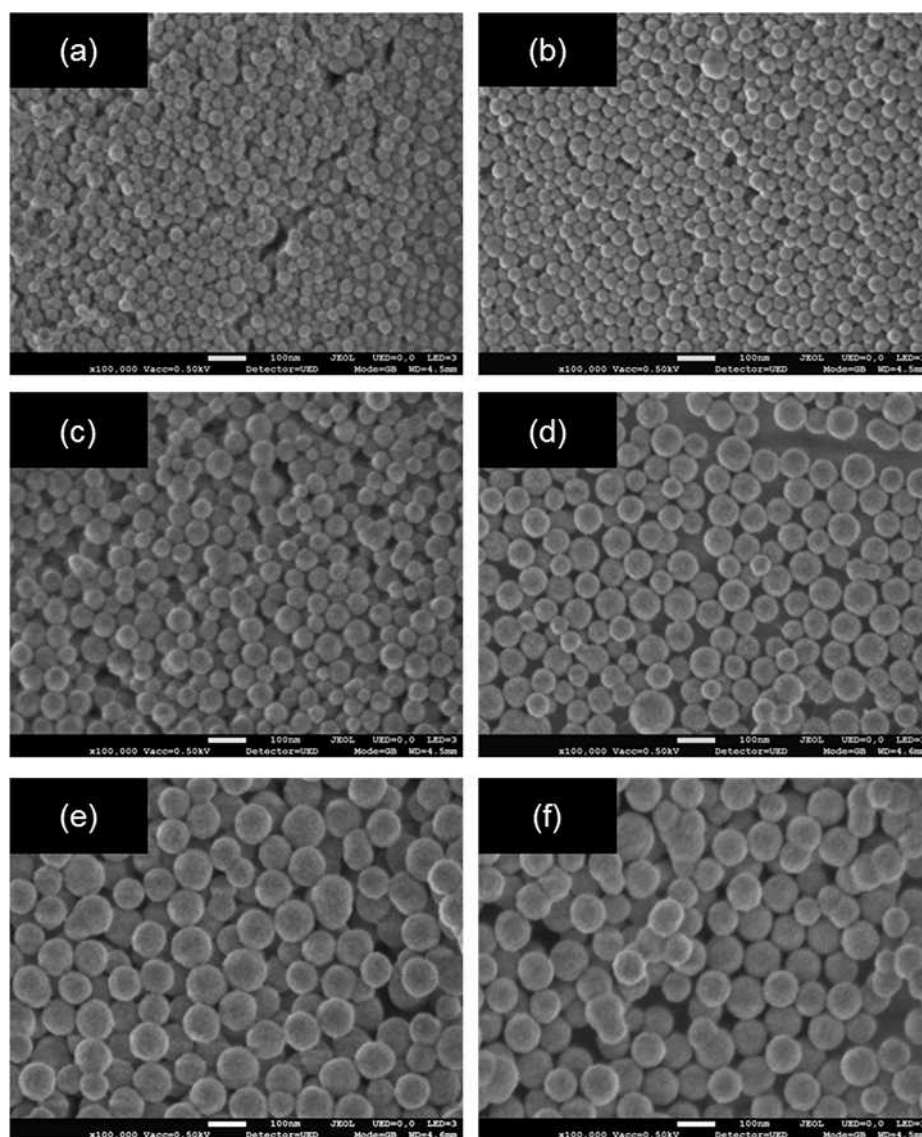


Fig. 4-5 SEM images of porous silica particles from sample 12 at various reaction times: (a) 5, (b) 10, (c) 30, (d) 60, (e) 120 and (f) 140 min.

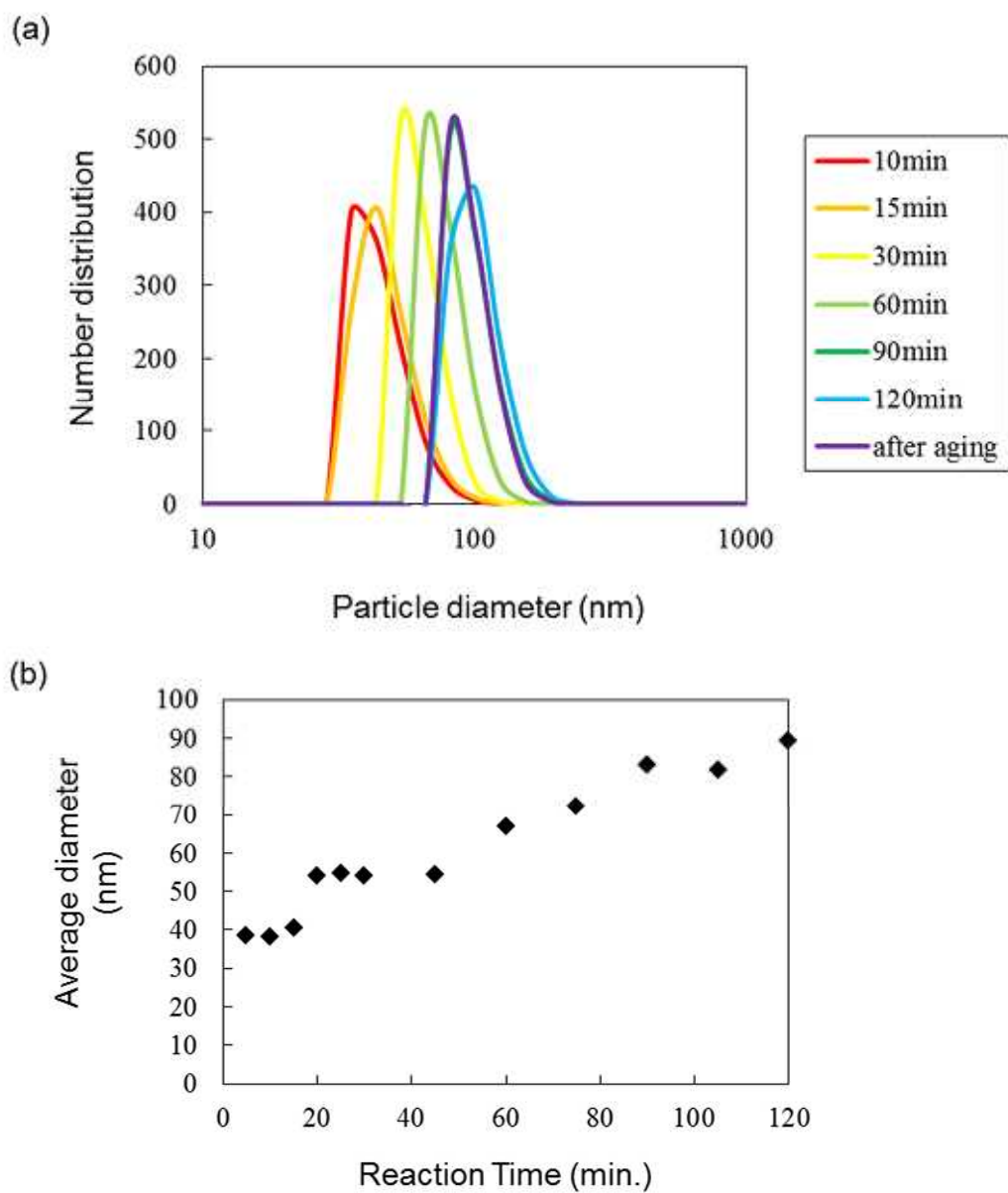


Fig. 4-6 DLS measurements of sample 12: (a) number distribution; and (b) average diameter of porous silica particles with reaction time (5–120 min).

4.4. Conclusion

The effect of template molecules on the particle morphology of monodispersed and microporous silica particles via gradual injection of reactants was investigated. Ammonium salts were found to be useful for synthesizing porous silica with a large SSA value because of their strong interaction with silica species. The use of primary amines is key to controlling the porosity and morphology. Furthermore, the use of amines with a good solubility in the reaction solution ($\log P_{ow} < 7$) enables the preparation of monodispersed silica particles with diameters of 100 nm whose SSA can be tuned in the range of 40–530 m²/g. Among such amines, the use of DA as a templating agent is effective for the synthesis of monodispersed silica particles 100 nm in diameter and 530 m²/g in SSA. These results indicate that the present synthesis method is suitable for the large-scale synthesis of monodispersed and microporous silica particles with a variety of SSAs.

References

1. C. Barbé, J. Bartlett, L. Kong, K. Finnie, H. Q. Lin, M. Larkin, S. Calleja, A. Bush and G. Calleja, *Adv. Mater.*, 2004, **16**, 1959–1966.
2. J. Lu, M. Liang, J. I. Zink and F. Tamanoi, *Small*, 2007, **3** (8), 1341–1346.
3. M. Liang, J. Lu, M. Kovoichich, T. Xia, S. G. Ruehm, A. E. Nel, F. Tamanoi and J. I. Zink, *ACS Nano*, 2008, **2** (5), 889–896.
4. F. Lu, S. -H. Wu, Y. Hung and C. -Y. Mou, *Small*, 2009, **5** (12), 1408–1413.
5. X. Du and J. He, *Nanoscale*, 2011, **3**, 3984–4002.
6. C. Urata, H. Yamada, R. Wakabayashi, Y. Aoyama, S. Hirose, S. Arai, S. Takeoka, Y. Yamauchi and K. Kuroda, *J. Am. Chem. Soc.*, 2011, **133**, 8102–8105.
7. H. Yamada, C. Urata, Y. Aoyama, S. Osada, Y. Yamauchi and K. Kuroda, *Chem. Mater.*, 2012, **24**, 1462–1471.
8. Y.-S. Lin, K. R. Hurley and C. L. Haynes, *J. Phys. Chem. Lett.*, 2012, **3**, 364–374.
9. P. Yang, S. Gaib and J. Lin, *Chem. Soc. Rev.*, 2012, **41**, 3679–3698.
10. S. Kwon, R. K. Singh, R. A. Perez, E. A. A. Neel, H.-W. Kim and W. Chrzanowski, *J.*

- Tissue Eng.*, 2013, **4**, 1–18.
11. B. G. Prevo, Y. Hwang and O. D. Velev, *Chem. Mater.*, 2005, **17**, 3642–3651.
 12. J. Kobler and T. Bein, *ACS Nano*, 2008, **11**, 2324–2330.
 13. Y. Hoshikawa, H. Yabe, A. Nomura, T. Yamaki, A. Shimojima and T. Okubo, *Chem. Mater.*, 2010, **22**, 12–14.
 14. K. Katagiri, S. Yamazaki, K. Inumaru and K. Koumoto, *Polymer Journal*, 2015, **47**, 190–194.
 15. R. I. Nooney, D. Thirunavukkarasu, Y. Chen, R. Josephs and A. E. Ostafin, *Chem. Mater.*, 2002, **12**, 4721–4728.
 16. K. Ikari, K. Suzuki and H. Imai, *Langmuir*, 2004, **20**, 11504–11508.
 17. K. Suzuki, K. Ikari and H. Imai, *J. Am. Chem. Soc.*, 2004, **126**, 462–463.
 18. K. Ikari, K. Suzuki and H. Imai, *Langmuir*, 2006, **22**, 802–806.
 19. K. Yano, N. Suzuki, Y. Akimoto and Y. Fukushima, *Bull. Chem. Soc. Jpn.*, 2002, **75**, 1977–1982.
 20. K. Yano and Y. Fukushima, *J. Mater. Chem.*, 2003, **13**, 2577–2581.
 21. K. Yano and Y. Fukushima, *J. Mater. Chem.*, 2004, **14**, 1579–1584.
 22. Y. Yamada and K. Yano, *Micro. Meso. Mater.*, 2006, **93**, 190–198.
 23. M. Mizutani, Y. Yamada, T. Nakamura and K. Yano, *Chem. Mater.*, 2008, **20**, 4777–4782.
 24. K. Yano, M. B. Katz, X. Pan and N. Tatsuda, *J. Colloid Interface Sci.*, 2014, **418**, 61–65.
 25. C. Urata, Y. Aoyama, A. Tonegawa, Y. Yamauchi and K. Kuroda, *Chem. Commun.*, 2009, **34**, 5094–5096.
 26. H. Yamada, C. Urata, H. Ujiie, Y. Yamauchi and K. Kuroda, *Nanoscale*, 2013, **5**, 6145–6153.
 27. K. Kuroda, A. Shimojima, K. Kawahara, R. Watabayashi, Y. Yamura, Y. Asakura and M. Kitahara, *Chem. Mater.*, 2014, **26**, 211–220.
 28. K. Möller, J. Kobler and T. Bein, *Adv. Funct. Mater.*, 2007, **17**, 605–612.
 29. Z.-A. Qiao, L. Zhang, M. Guo, Y. Liu and Q. Huo, *Chem. Mater.*, 2009, **21**, 3823–3829.
 30. K. Zhang, L. L. Xu, J. G. Jiang, N. Calin, K. F. Lam, S. J. Zhang, H. H. Wu, G. D. Wu, B. Albela, L. Bonneviot and P. Wu, *J. Am. Chem. Soc.*, 2013, **135**, 2427–2430.

31. S. -H. Wu, C. -Y. Mou and H. -P. Lin, *Chem. Soc. Rev.*, 2013, **42** (9), 3862–3875.
32. T. Shimogaki, H. Tokoro, M. Tabuchi, N. Koike, Y. Yamashina and M. Takahashi, *J. Sol-Gel Sci. Technol.*, 2015, **74**, 109–113.
33. W. Stöber and A. Fink, *J. Colloid Interface Sci.*, 1968, **26**, 62–69.
34. T. Shimogaki, H. Tokoro, M. Tabuchi, N. Koike, Y. Yamashina and M. Takahashi, *J. Sol-Gel Sci.*, 2015, **76**, 156–163.
35. C. J. Brinker and G. W. Scherer, *Sol-Gel Science: The Physics and Chemistry of Sol-Gel Processing*; Academic Press: Boston, 1990.

Chapter 5

Single- Process Fabrication of Antireflective Acrylic Hard Coating via Surface Segregation of Porous Silica Nano- Particles

5.1 Introduction

Antireflective (AR) coatings are an important class of technology used to improve the quality of our daily life by offering a better visibility for flat panel displays, mobile phones and tablets by reducing the reflection of surrounding light [1–3]. Two types of AR coating have been reported and industrialized so far. The optical reflection is suppressed by surface microstructures or coatings with a refractive index between the window materials and air, which decreases the refractive index contrast at the air interface [4–21]. Another type of AR coating is designed to cancel the optical reflection by optical interference within the multilayers of alternating refractive indexes [22–24]. A typical example of the former AR surface is the moth's eye structure [10–16, 25]. This structure mimics the eyes of moths, in which micro cones ~100 nm in diameter and several hundreds of nm in height with 100 to 200 nm regular spacings are fabricated on the entire surface of the display devices. The refractive index of the moth's eye surfaces gradually changes from that of air to that of the window material. The optical reflection is suppressed because of the absence of a refractive index jump at the interfaces. The moth's eye structure shows an excellent AR capability. However, the sophisticated lithographic technique at the 100 nm scale is required to fabricate the moth's eye structure. In addition, such micro structures are very fragile and do not survive mechanical contact by human fingers or other objects. Furthermore, the substrate is limited to hard materials such as glass because they need to be capable of nanolithography. Further improvement in mechanical robustness is strongly required for moth's eye-structured AR surfaces. The multilayer optical thin film is widely used for displays or glasses presently available because of their simple structure and better surface mechanical properties [22–24]. The use of the porous silica nano-particles as AR coating is also reported by several literatures [18, 20, 21]. By preparing an optical thin film with a designated refractive index and thickness, the two reflections at the air/film and film/device interfaces interfere each other, resulting in the cancelation of the reflection of light through an anti-phase interaction. Low-refractive index coatings are usually required for this type of AR coating. However, the low refractive index layer is required to be coated at a thickness of 100 nm with an accuracy of several nanometers, which is technologically very difficult from an industrial point of view. In addition, the properties of this type of AR coating exhibit a strong dependence

on the incidence angle. In addition, the size of displays are increasing day by day, but their thickness and weight are decreasing, so the surface materials of displays are replacing from glass to hard coat resins. Roll-to-roll process is practically used for such large-sized coating. Therefore, an easier and simpler method for robust resin AR coatings for large area exceeding several tens to hundreds inches is strongly required from both industrial and practical points of view.

In this Chapter, a hard coating acrylic polymer film with a surface-segregated porous silica nano-particle layer by a single bar-coating process which can be easily transformed into a roll-to-roll fabrication has been proposed as a new type of AR coating possessing mechanical robustness coupled with excellent optical quality. The surface porous silica layer embedded in the resin serves as a surface low-refractive index layer that does not deteriorate and demonstrates the mechanical robustness of a polymer hard coating. One of the advantages of the present approach is that the substrate materials are not limited, which means they can be used for variety of applications. In addition, such composite films can be formed via a single coating process. The surface porous silica particle layer is formed through spontaneous self-organization during the coating process. When the surface free energy of silica particles is lower than that of acrylic monomers, which can be considered a polymer hard coating, the particles will eventually segregate on the polymer/air interface to minimize the interfacial energy. The surface tension of acrylic monomers is in the range of 30 to 50 mN/m [26]. By optimizing the surface chemistry of nano silica particles, single-layered homogeneous segregation can be formed at the polymer/air interface. A conceptual schematic of the present approach is depicted in Fig. 5-1. It is difficult to control such surface segregation with bare silica particles because the surface silanol group has a high polarity and a large surface free energy (>100 mN/m). Reducing the surface energy of the silica particles is required to induce the segregation at the polymer/air interface. The surface energy of the porous silica nano-particles can be reduced by grafting a perfluoroalkyl group on the surface. The trifluoromethyl group (CF_3) in perfluoroalkyl shows the lowest critical surface tension (6 mN/m) among organic functional groups. The particles modified with a CF_3 group are expected to segregate at the air interface to minimize the interfacial energy. Recently, however, the use of fluoro-compounds has been greatly limited because of some

concerns for the safety of the human body and environment. Therefore, the use of non-fluorinated surface grafting agents to adjust the surface energy is required. The surface energy of a methyl group has been reported to be 22 to 24 mN/m [27, 28], so that grafting agents with methyl groups on a silica surface decreases the surface energy below that of acrylic monomers.

In this Chapter, porous silica particles were modified with hexamethyldisilazane (HMDS). To investigate the relationship between the silica coverage factor of HMDS and the tendency of surface segregation, acrylic hard coatings containing modified porous silica nano-particles with various surface coverages were prepared. Hollow nano silica particles were also used for comparison. The uniform segregation of porous silica particles at the air interface was carefully monitored to achieve a new type of AR hard coating.

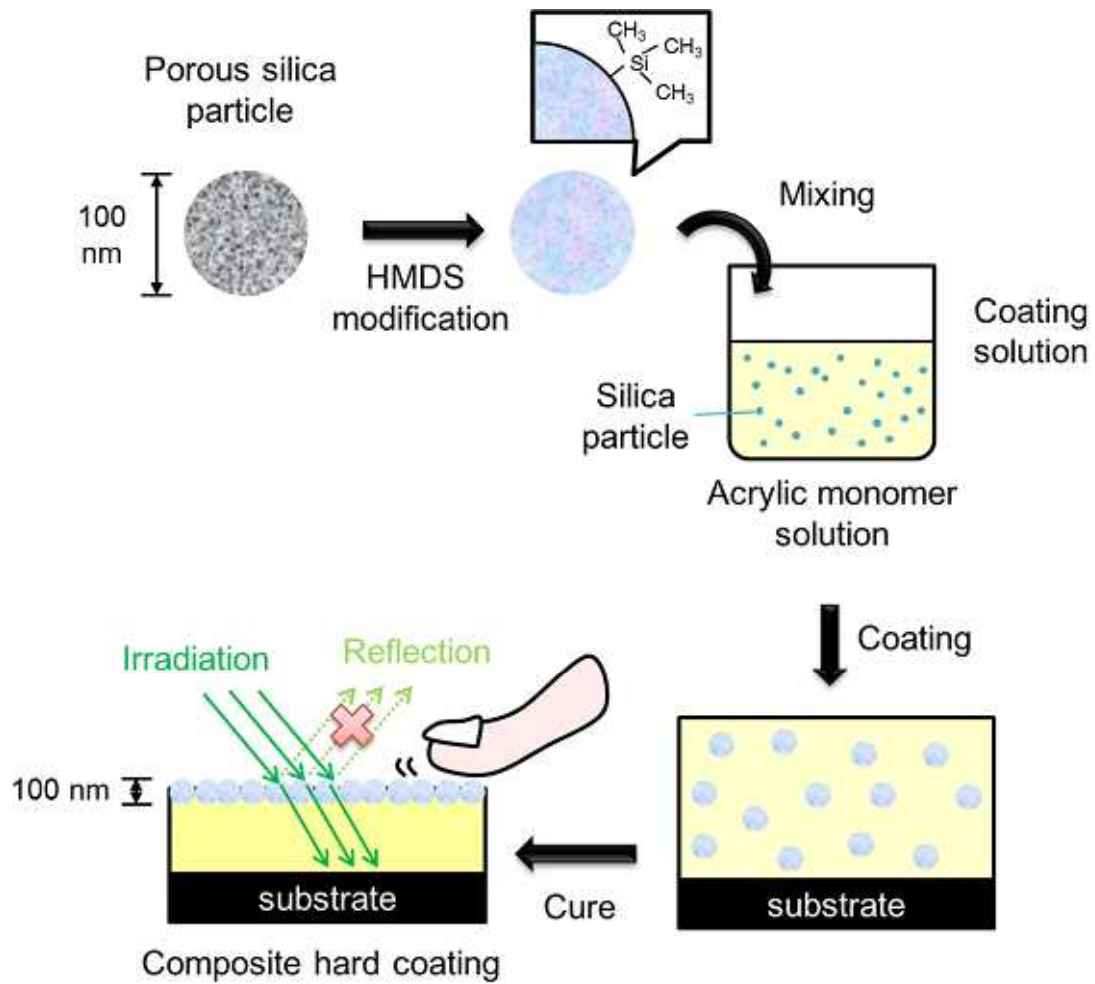


Fig. 5-1 Conceptual scheme of the present approach.

5.2. Experimental

5.2.1 Materials

Methanol (Kanto Chemical Co. Inc., Japan), 2-propanol (IPA; Kanto Chemical Co. Inc., Japan), methyl ethyl ketone (MEK; Kanto Chemical Co. Inc., Japan), tetramethoxy orthosilicate (TMOS; Shin-Etsu, Japan), n-dodecylamine (DDA; TCI, Japan), n-decylamine (DA; TCI, Japan), 28 % aqueous ammonia (NH₃, Wako Inc., Japan), acetic acid (TCI, Japan), hexamethyldisilazane (HMDS; TCI, Japan), Nano Balloon XL100 (hollow silica spheres, GRANDTEX, Japan), ARONIX M-306 (acrylic hard coating monomer: mixture of pentaerythritol triacrylate and pentaerythritol tetraacrylate, TOAGOSEI Co., LTD., Japan), IRGACURE 184 (photo initiator, BASF Canada Inc., Canada), and MEGAFACE F-444 (DIC, Japan) were used as received.

5.2.2 Synthesis

Preparation of mesoporous silica particle.

Mesoporous silica particles were prepared using a procedure reported in Chapter 2–4 [29–31]. Methanol (852.8 g), distilled water (245.2 g), and 28 % NH₃ (109.6 g) were mixed in a 2 L four-neck flask at 20 °C. Methanol (180.4 g), DA (127.6 g), and TMOS (137.2 g) were mixed in a polyethylene (PE) container and were then injected into the first flask with a tube pump for 120 min under vigorous stirring. The molar ratio of the reaction solution was TMOS/DA/NH₃/H₂O = 0.5/0.4/1/10. The reaction solution was stirred for another 1 h after completion of the injection. The resulting precipitates were collected by centrifugation and dried at 120 °C in air for 2 h, and calcined in air at 600 °C for 6 h to remove DA. (yield: 50.6 g). The diameter and specific surface area of the resultant silica particles were 100 nm and 530 m²/g, respectively. The pore volume was 0.18 cm³/g, with an estimated pore volume of ca. 30 %.

Experiments shown in Figs. 5–12 and 5–13 were carried out with silica particles prepared with a different chemical composition. Methanol (852.8 g), distilled water (245.2 g), and 28 % NH₃ (109.6 g) were mixed in a 2 L four-neck flask at 20 °C. Methanol (180.4 g), DDA (37.1 g), and TMOS (137.2 g) were mixed in PE container, and were then injected into the first flask with a tube pump for 120 min under vigorous stirring. The molar ratio of the reaction

solution was $\text{TMOS/DDA/NH}_3/\text{H}_2\text{O} = 0.5/0.1/1/10$. The reaction solution was stirred for another 1 h after completion of the injection. The resulting precipitates were collected by centrifugation and dried at 120 °C in air for 2 h, and calcined in air at 600 °C for 6 h to remove DDA. (yield: 48.9 g). They were 100 nm in diameter and had a specific surface area of 100 m²/g. The pore volume was 0.04 cm³/g, with an estimated pore volume of ca. 10 %.

Surface modification of mesoporous silica particles.

The obtained silica particles (5.0 g) were dispersed in IPA (44.5 g) containing acetic acid (0.5 g) and a prescribed amount of HMDS under ultra-sonication and then a wet jet mill (Nano Jet Pal JN 20, JOKOH, Japan). The resultant dispersion of silica particles was refluxed at 82 °C to complete the surface grafting reaction. Precipitates were collected by centrifugation and dried at 100 °C in air for 2 h. The surface modification by HMDS was confirmed by the existence of a peak at approximately 14 ppm by ²⁹Si-NMR spectroscopy and thermal gravity analysis.

5.2.3 Coating

The modified silica particles (5 g) were dispersed in IPA (45 g). The obtained dispersion (50 g), ARONIX M-306 (100 g) as a poly acrylic monomer, and IRGACURE 184 (5 g) as a photo initiator were mixed in MEK (120 g). The obtained coating solution was coated with a #18 bar coater on PET films and dried at 80 °C for 2 min. Then this film was irradiated with 250 mJ of UV light.

5.2.4 Characterization

Scanning electron microscope (SEM) images were obtained using a JSM-7500TFE microscope (JEOL Ltd., Japan), at an accelerating voltage of 0.5 kV. Transmission electron microscope (TEM) images were obtained using a JEM-2200FS microscope (JEOL Ltd.), at an accelerating voltage of 200 kV. Optical reflection spectra (angle of incidence = 5°) were measured with air as the reference using a UV–visible spectrometer U-4100 (Hitachi High-Tech, Japan). Haze and total light transmittance were measured with an ND2000 haze meter (Nippon

Denshoku Industries Co., LTD, Japan).

5.3. Results and Discussion

5.3.1 Surface Modification

Microporous and monodispersed silica nano-particles 100 nm in diameter were synthesized following the procedure that I have reported in Chapter 2–4 [29–31]. Commercial hollow silica particles 50 to 60 nm in diameter (Nano Balloon XL100) were used for a comparison. Porous or hollow silica particles are considered to be the most suitable candidates for surface particle layers. However, bare silica particles show a poor affinity with acrylic monomers/resins because of their strong cohesion force and large difference in surface energy. For example, the critical surface tensions of silica particles and general acrylic monomers are >100 mN/m and 30 to 50 mN/m, respectively. It is thus necessary to modify the surface of silica particles by grafting molecules with a lower surface energy while maintaining good affinity with the surrounding media. HMDS was selected as the grafting molecules to reduce the surface energy of the particles. If the entire surface of silica particles is covered with CH_3 , the critical surface tension becomes 22 to 24 mN/m [27, 28]. For hollow silica particles, the particles were broken by a large shear force during the wet jet milling process (Fig. 5–2). Even though hollow silica particles seem to be the best candidate material for the surface layer because of their small refractive index, their decreased mechanical stability makes them unusable for the present purpose. Accordingly, the following experiments were carried out only with the microporous silica particles.

By surface modification of microporous silica particles, micro pores might be filled with HMDS. The relationship between the theoretical coverage of HMDS and the pore volume of the modified silica particles is shown in Fig. 5–3. The theoretical coverage was calculated using equation (1):

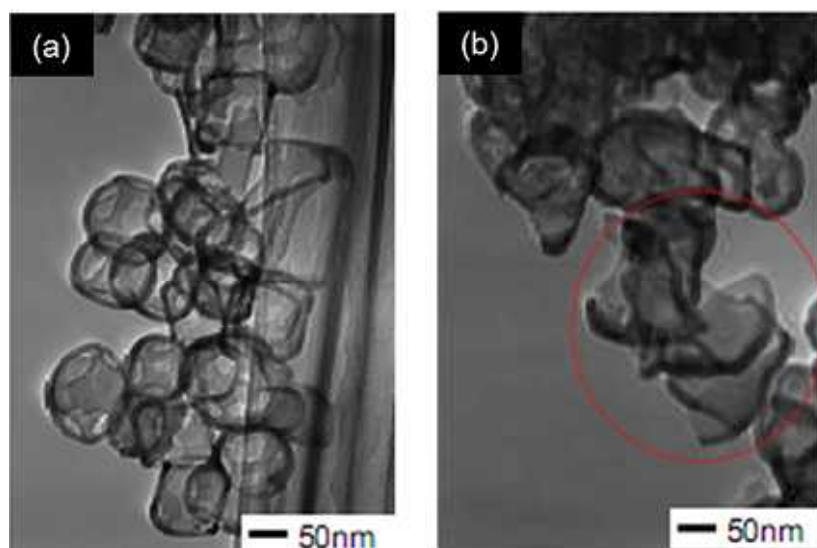


Fig. 5-2 The TEM images of hollow silica particles (a) before and (b) after jet mill process. Red circle indicates the broken particles.

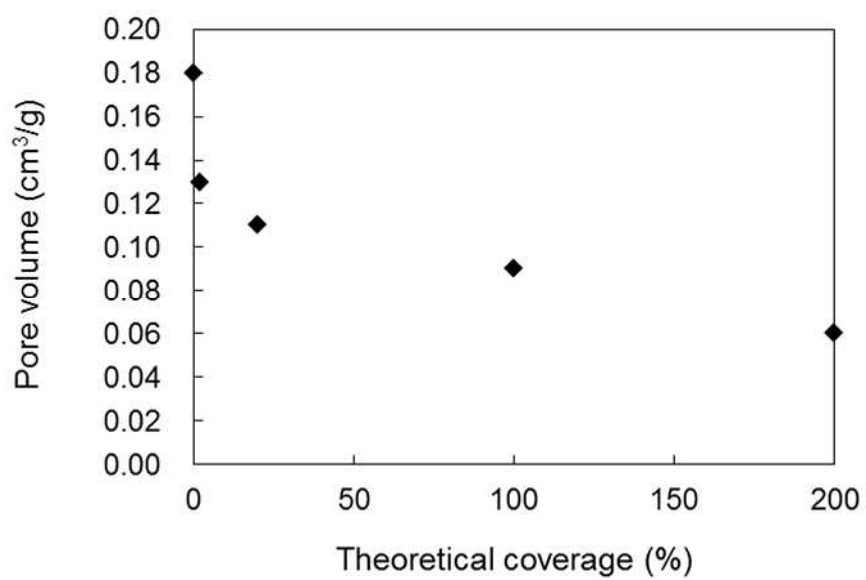


Fig. 5-3 Relationship between theoretical coverage of microporous silica particles modified with various amount of HMDS and measured pore volume.

$$\textit{theoretical coverage} (\%) = \frac{[\textit{theoretical area of HMDS molecule (m}^2/\textit{g)}] \times [\textit{amount of HMDS (g)}]}{[\textit{sprcific surface area of silica (m}^2/\textit{g)}] \times [\textit{amount of silica (g)}]} \times 100$$

(1)

The theoretical coverage area of the HMDS molecule is assumed to be 967 m²/g [32], and the amount of HMDS is experimentally estimated by measuring the consumed quantity of HMDS during the surface modification process. The pore volume of porous silica decreased with the surface coverage, in other words, with increasing amounts of HMDS. It should be noted that the HMDS modifies not only the outermost surface of silica particles but also inside the pores. In the case of particles with 100 % coverage of HMDS, the pore volume decreased to half that of bare particles. Practical amount of HMDS grafting on the surface of nano silica is hardly quantified, but thermal gravity analyses indicate the larger amount of HMDS are grafted for porous silica with higher the theoretical area (Fig. 5–4). The weight loss is not linear to the theoretical coverage, but the porous silica of larger the theoretical coverage exhibit more weight loss. The weight loss is mainly due to the burning out of HMDS. A small loss observed for 0 % coverage is considered to be due to the water condensation of residual silanols.

5.3.2 Coating

The IPA-MEK acrylic monomer solution of ARONIX M-306 and IRGACURE 184 containing silica particles modified with various amount of HMDS was coated on PET film substrates by bar-coating to determine the surface segregation tendency. ARONIX M-306 contains pentaerythritol triacrylate and pentaerythritol tetraacrylate monomers (PETA), which is known to be one of the general multifunctional acrylic resins for hard coatings (Fig. 5–5).

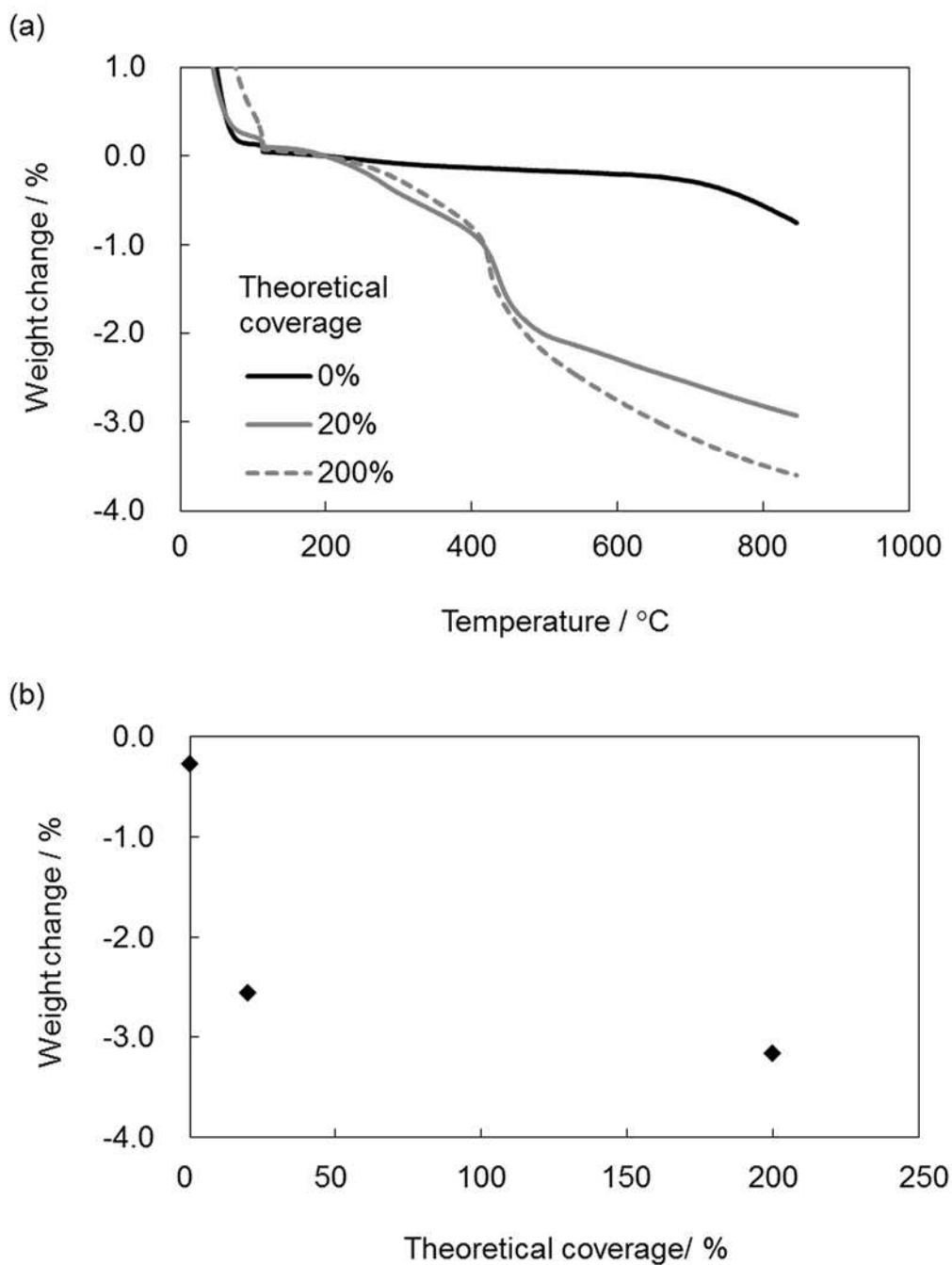


Fig. 5-4 Thermal gravimetric analysis (TGA) of HMDS modified porous silica particles. (a) TGA curves of theoretical coverage of 0 %, 20 % and 200 %, here the weight loss is normalized at 200 °C. (b) Weight loss of 200 °C to 800 °C.

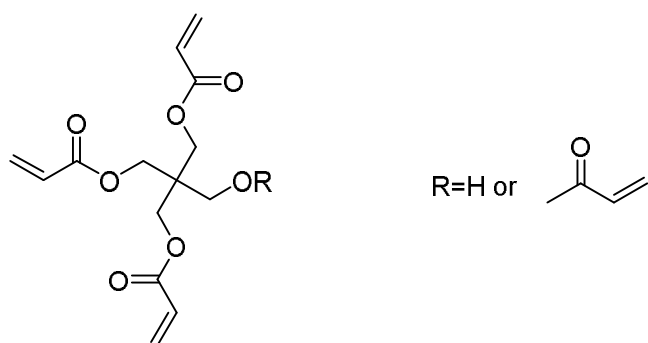


Fig. 5-5 Molecular structures of ARONIX M-306.

Cross-sectional TEM and surface SEM images of coating films are shown in Figs. 5–6 and 5–7, respectively. AFM images of the surface of coating films and their haze are shown in Fig. 5–8. The non-modified silica particles are dispersed almost homogeneously in the hard coating (Fig. 5–6 (a)). However, the modified particles exhibit single-layer segregation of silica particles at the air interface (Fig. 5–6 (b) and (c)), leaving a certain fraction of the particles on the interior of the films. In TEM images, the amount of surface segregation is almost the same for HMDS coverages of 20 and 100 %, where the rates of particles segregation at the air interface were ca. 40 % in both cases. In contrast, the rate of bare particles is 4 %. A 20 area% coverage of HMDS on silica particles seems to be sufficient for the formation of the surface segregated layer. With the present approach, the surface layer of silica nano-particles can be spontaneously formed through the segregation via a surface energy mismatch between the particles and the acrylic monomers. As a result, the air interface is almost completely covered by a single layer of silica nano-particles.

The theoretical AR capability of the present system was examined by theoretical simulation (Figs. 5–9 and 5–10). Using silica particles with 40 and 50 % pore volume, the reflectance was calculated to be less than 1 %. In other words, the present coatings show great potential as AR coatings. The AR property of these films was also experimentally examined. Reflectance spectra were measured for samples prepared with silica nano-particles with various surface coverages of HMDS (Fig. 5–11). The reflectance at 550 nm, which is a highly visible wavelength, and total light transmission are shown in Table 5–1. All films showed >90 % transmission, which is sufficiently transparent for display applications. Furthermore, the pencil hardness of these films were H~3H, even on PET film as a substrate, demonstrating that these films are highly scratch-resistant, similar to the acrylic coating without silica particles. The reflectance of films with a silica particle layer was <3 %, lower than that of the film with bare silica particles (4.1 %). The reflectance of the film containing porous silica particles with 100 area% coverage of HMDS is larger than the theoretical prediction. This may be due to the in-plane inhomogeneity of the surface silica layer and reduction of the pore volume by HMDS modification, which could be further improved by optimization.

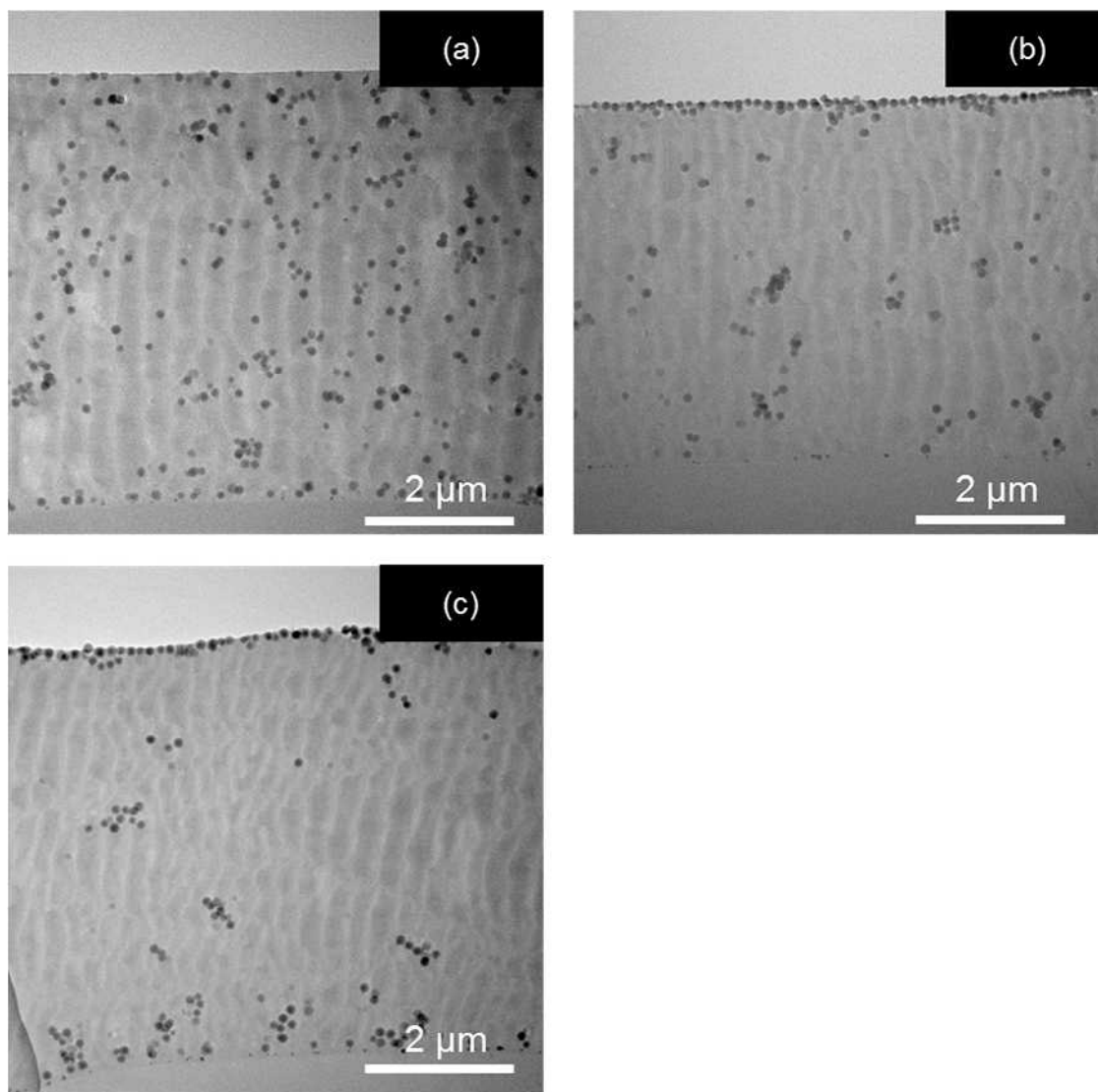


Fig. 5-6 Cross sectional TEM images of coating films containing porous silica particle with various surface coverages of HMDS; (a) 0, (b) 20 and (c) 100 area%.

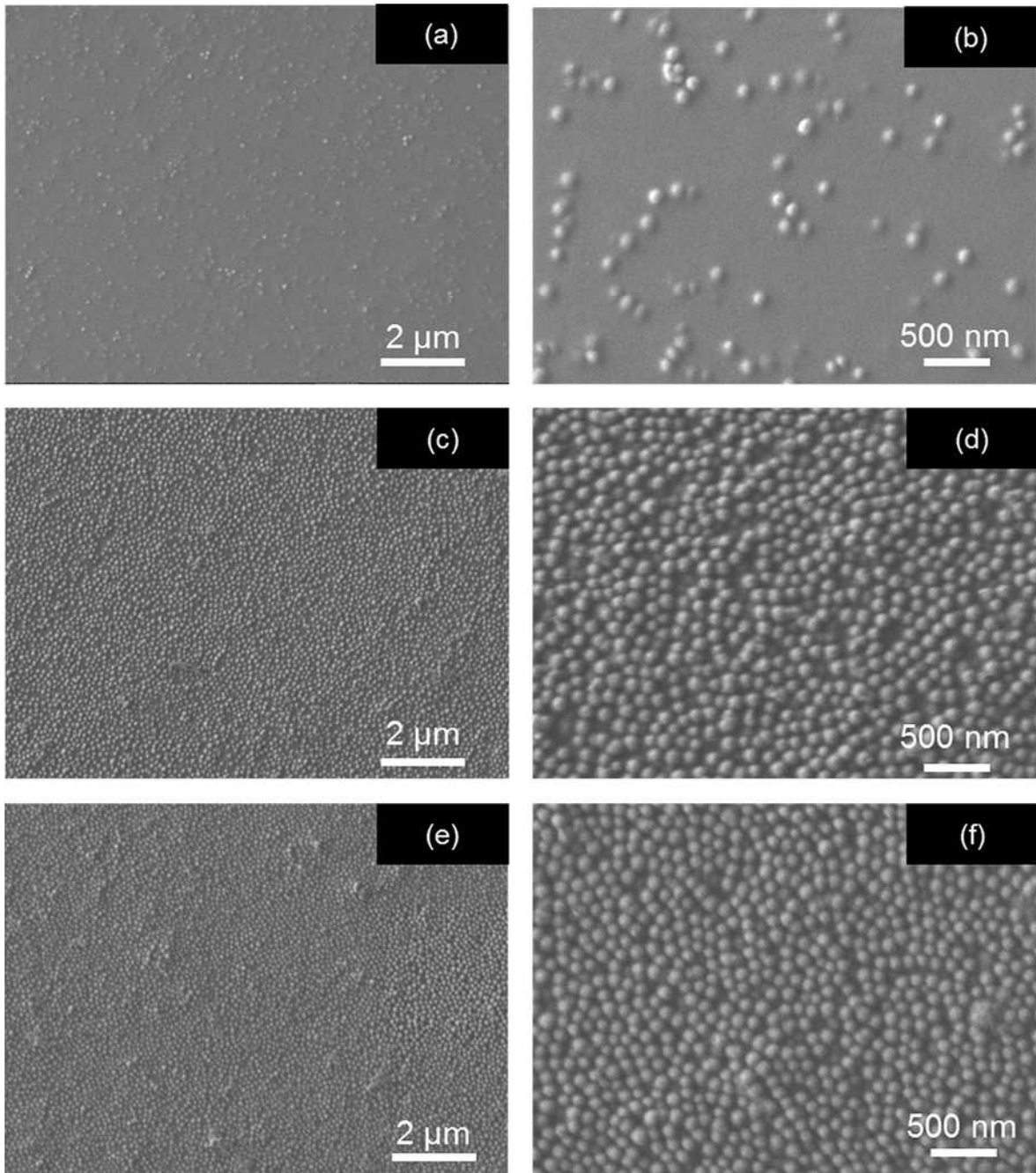


Fig. 5-7 SEM images of the surface of coating films containing porous silica particle with various surface coverages of HMDS; (a, b) 0, (c, d) 20 and (e, f) 100 area%.

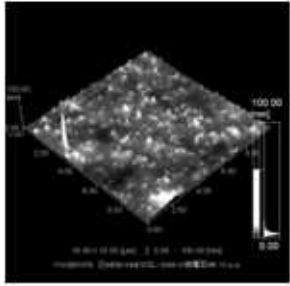
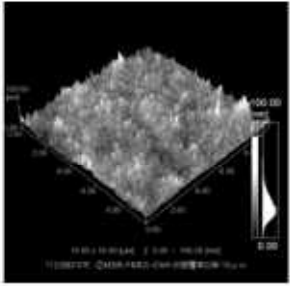
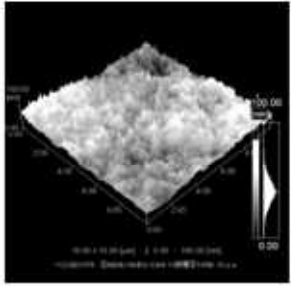
Theoretical coverage (%)	0	20	100
AFM Images			
Ra (nm)	2.6	8.9	12.0
HAZE	1.34	1.39	1.79

Fig. 5-8 AFM images, surface roughness (Ra) and HAZE of surface of coating film containing porous silica particle modified with HMDS (a) 0, (b) 20 and (c) 100 area%.

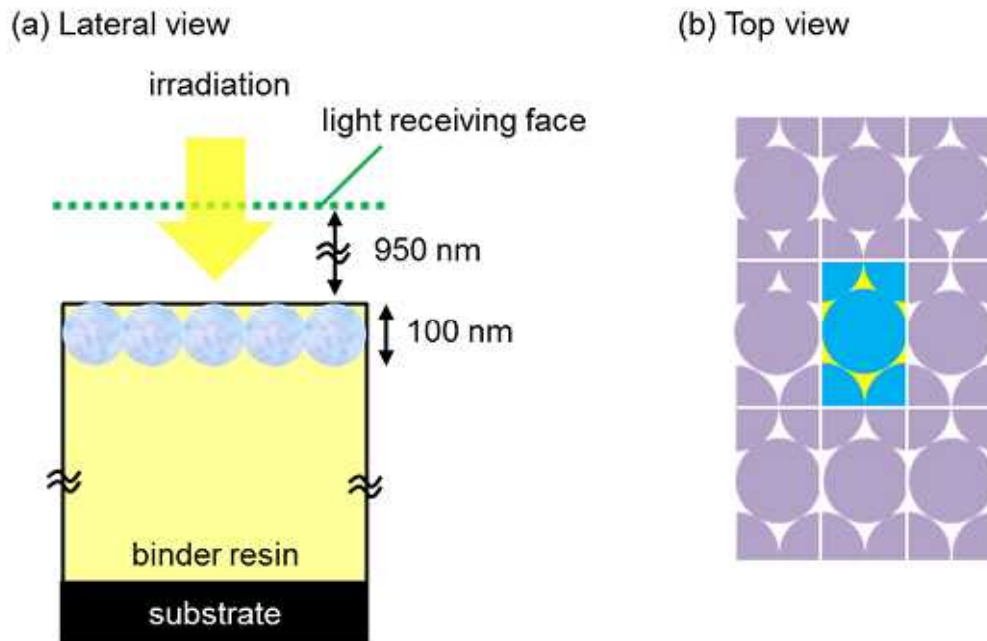


Fig. 5–9 Model diagrams of optical simulation of reflectance spectra of the present AR films constituting of segregated silica layer calculated by Finite-Difference Time-Domain (FDTD) method (K.S. Yee: "Numerical Solution of Initial Boundary Value Problems Involving Maxwell's Equations in Isotropic Media", IEEE Trans. AP-14, pp.302–307 (1966)); (a) a lateral view and (b) a top view. It was assumed that a diameter of the porous silica particle is 100 nm, refractive index of silica as 1.32 (pore volume of silica particle = 30 %), 1.27 (pore volume of silica particle = 40 %) or 1.22 (pore volume of silica particle = 50 %) and refractive index of binder resin as 1.50. The film thickness of binder resin was assumed enough large compared with the surface silica layer. The irradiation light is surface light source of vertical incidence. The distance between the light receiving face and surface of film is set to 950 nm. It is assumed the horizontal direction was replicated endlessly and silica particle is in the closed packing.

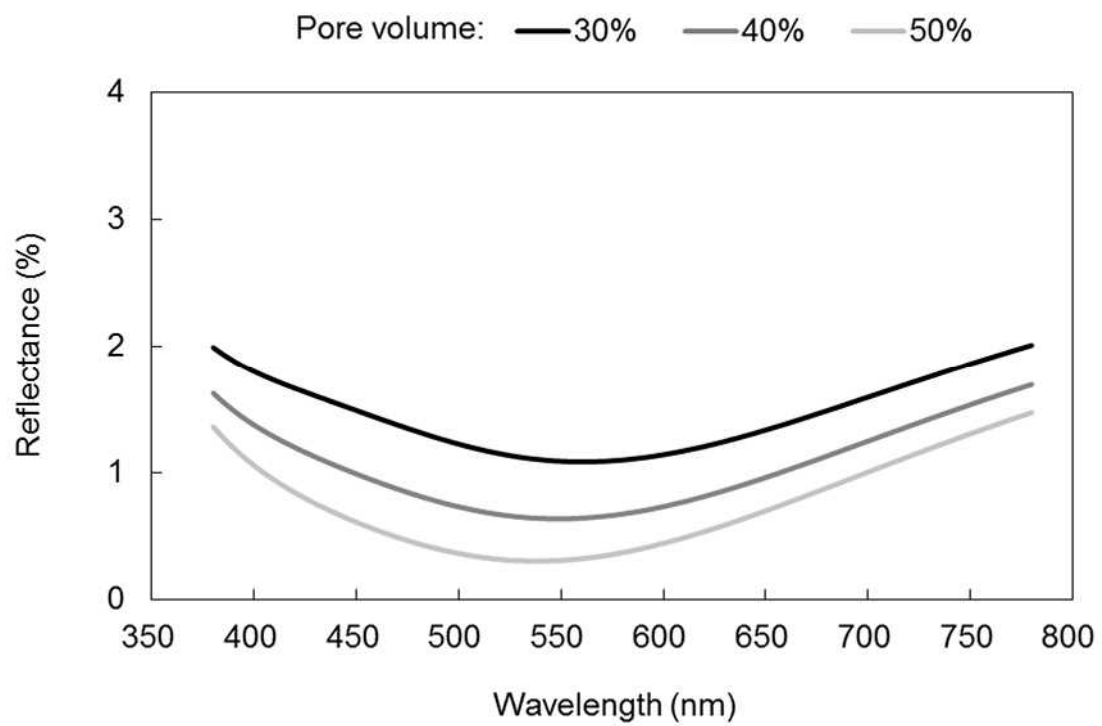


Fig. 5–10 Optical simulation of reflectance spectra using the model of Fig. 5–9 calculated by software “Poynting for Optic”.

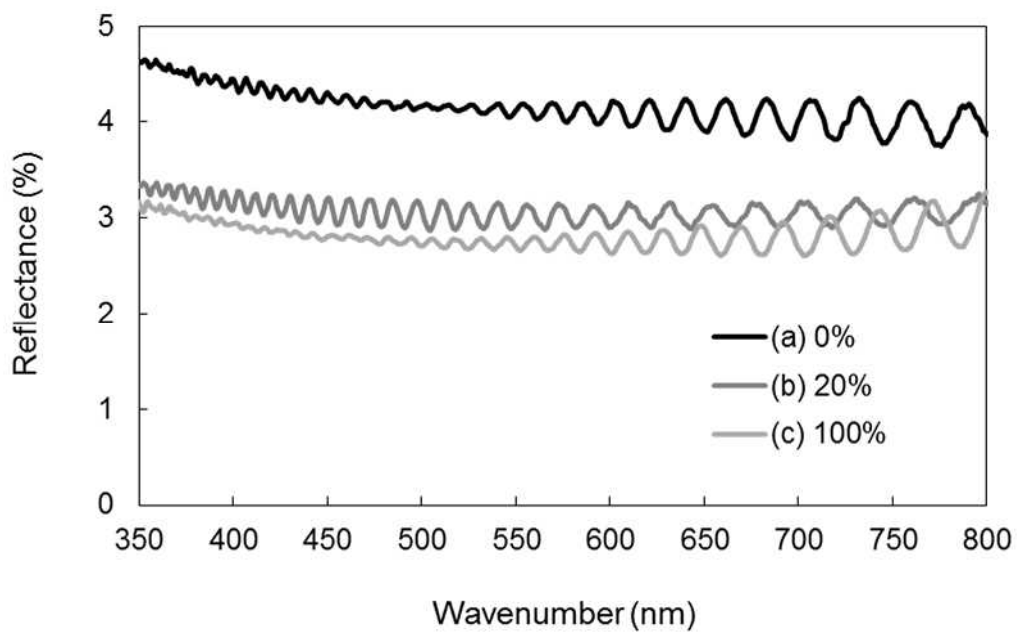


Fig. 5-11 Reflectance spectra of coating films containing silica particles modified by HMDS with a coverage of (a) 0, (b) 20, (c) 100 area%.

Table 5–1 Reflectance at 550 nm and total light transmission of AR films containing porous silica particles modified with various amount of HMDS.

Theoretical coverage (%)	0	20	100
Reflectance at 550 nm (%)	4.1	3.0	2.7
Total light transmission (%)	90.3	91.0	91.1

The reflectance of porous silica with 100 area% HMDS coverage showed a better AR property, 2.7%. However, the rate of segregation was the same as that of 20 area% HMDS coverage. Comparing SEM images of the surface of coating films, the 20 % coverage of HMDS on silica particles seems to have a rougher surface (inhomogeneous distribution of silica particles) (Fig. 5–7 (d)) than the one with 100 % coverage (Fig. 5–7 (f)). It was also observed that some of the particles seem to be stacked up. This inhomogeneity may influence the reflectance difference between films containing 20 and 100 area% modified with HMDS. These silica particles can be segregated easily at the air surface, reducing the optical reflection at the surface of the coating film.

The same experiments were carried out with silica particles of the same diameter but different porosity to see the effect of the density of the particles (Fig. 5–12). Even with silica particles with larger density (heavier than the previous experiments shown above), surface segregation of silica particles is achieved. Furthermore, in case of 15 wt.% silica particles containing system which containing 3 times more amount of silica particles than a coating film shown in Fig. 5–12 (a) , the silica particles formed only one layer, and the excessive silica particles were dispersed in coating resins instead of forming a second layer (Fig. 5–12 (b)).

To confirm the hypothesis that the segregation is due to the differences in the surface free energy, a fluoro-surfactant molecule (MEGAFACE F-554), the surface energy of which is lower than that of HMDS-modified silica particles, was incorporated into the acrylic monomer-silica particle solution (Fig. 5–13). It is expected that the fluoro-surfactant molecules will tend to accumulate at the air interface because of the large surface energy difference. In the

case of 1.0 wt.% fluoro-surfactant-containing film, the segregation of silica particles was no longer observed (Fig. 5–13 (b)). Even with 0.1 wt.% fluoro-surfactant addition, the number of surface silica particles drastically decreased compared with the cases shown in Fig. 5–6 (b) and (c). These observations indicate that, once the entire surface is covered by the single layer of silica particles or another surfactant with lower surface energy than silica particles, the remaining particles are immobilized in the matrix because of elimination of the air interface by the silica or the surfactant layer. This result also indicates that the surface segregation of silica particles is driven by the surface energy difference. The possibility of phase separation and buoyant force can be ruled out. Once the surface single layer of silica nano-particles formed, the segregation did not proceed further, resulting in the spontaneous formation of the silica particle single layer at the air interface. In addition, even if the excess amount of silica particles remains in the film matrix, they do not alter the optical transparency of the film because they are small compared with the wavelength of visible light.

To consider the segregation mechanism in more detail, the amount of solvent in the coating liquid was decreased from 60 to 50 and 45 wt.%. SEM images of the surfaces of the obtained coating films are shown in Fig. 5–14. As the amount of solvent decreased, the number of segregated silica particles decreased. This result indicates that the silica particles were segregated gradually under the convective flow during the dry coating process. Specifically, the silica particles were transferred to the air interface by convective flow. Once the silica arrived at the air interface, it was immobilized because the interface energy difference was unfavorable.

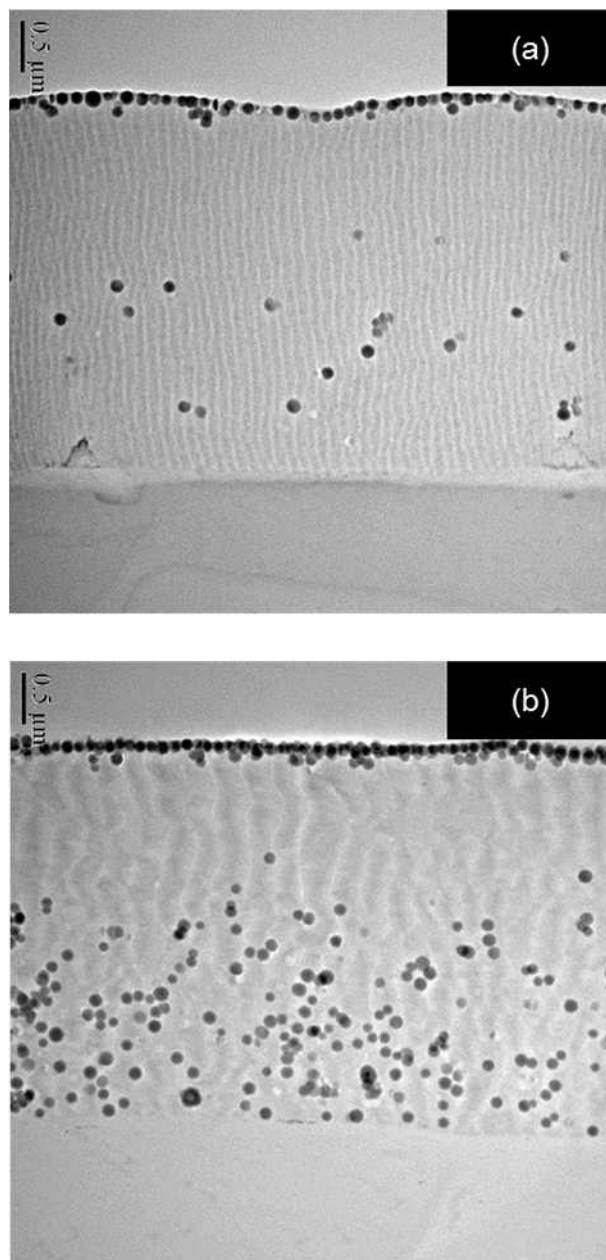


Fig. 5-12 TEM images of cross section of coating film containing (a) 5 and (b) 15 wt.% of porous silica particle, which the pore volume was $0.04 \text{ cm}^3/\text{g}$ and pore volume was estimated ca. 10 %.

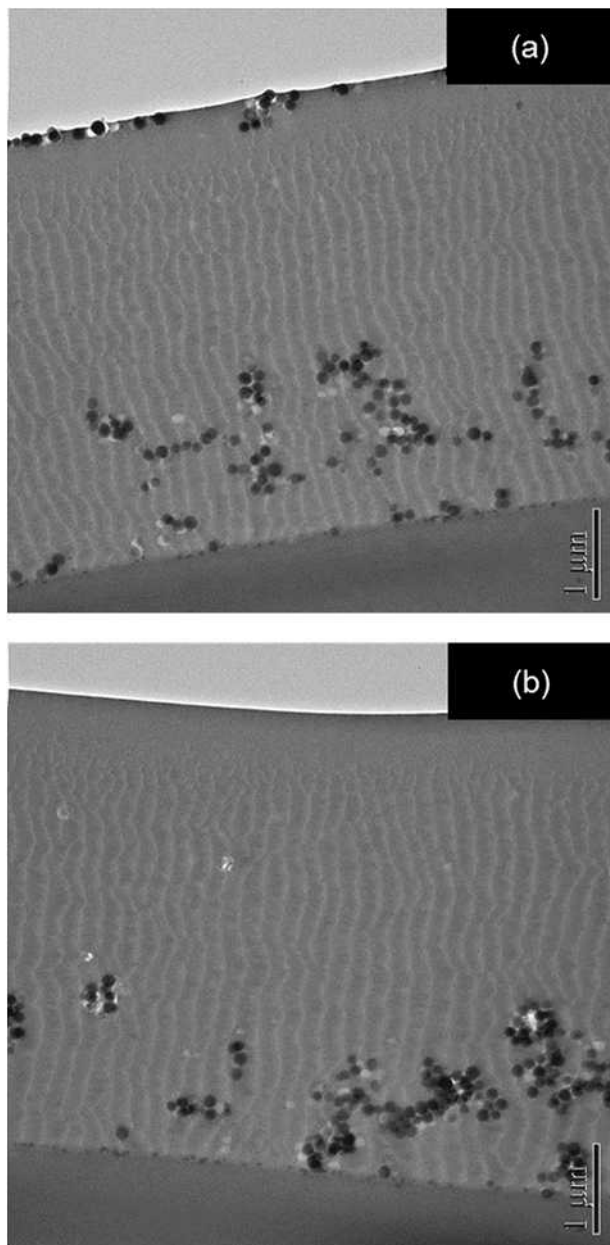


Fig. 5-13 TEM images of the cross section of coating films containing porous silica particle modified with HMDS and (a) 0.1 and (b) 1.0 wt.% fluoro-surfactant.

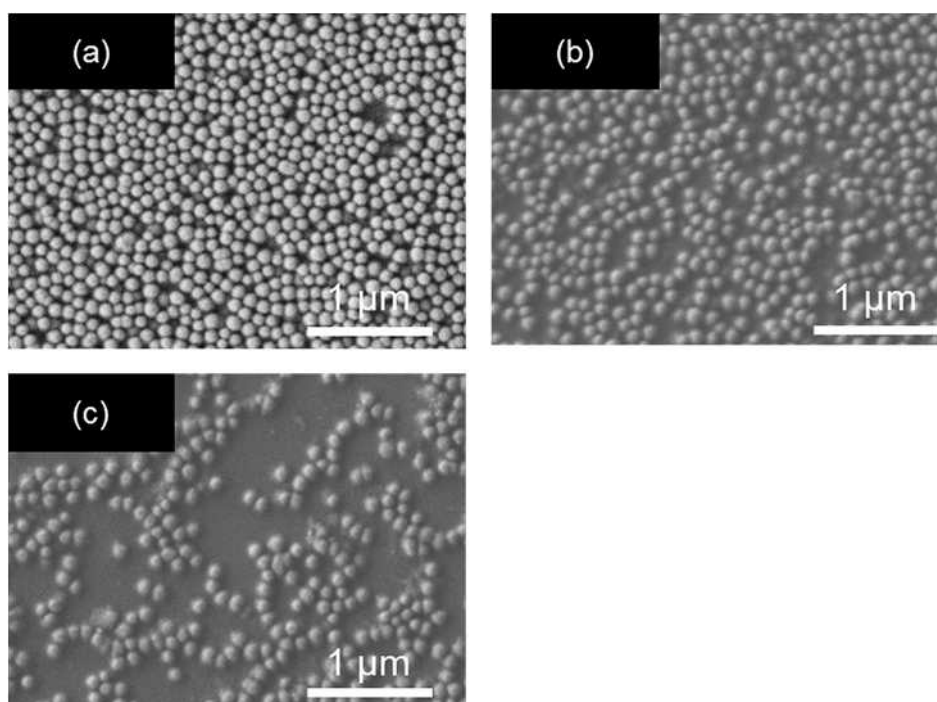


Fig. 5–14 SEM images of surfaces of coating film containing porous silica particles modified with HMDS; (a) 60, (b) 50 and (b) 45 wt.% solvent ratio.

5.4. Conclusion

Porous silica particles of 100 nm diameter with surfaces modified by HMDS can segregate spontaneously at the air surface to form a monolayer. The obtained hard-coating film shows AR properties. In this film, the monolayer of porous silica particles can form a low-refractive index layer. HMDS was found to be an effective modifier to segregate the particles at the air surface. One of the advantages of the present approach is that fluoro modifier is no longer required to adjust the surface energies. A reflectance of 2.7 % and pencil hardness of >H on a PET substrate were achieved. Another advantage is that the silica monolayer can serve as a low-refractive index 100-nm layer. The present approach offers an easier and simpler method for fabricating a robust AR coating for a variety of applications.

References

1. M. Ibn-Elhaj and M. Schadt, *Nature*, 2001, **410**, 796–799.
2. H. K. Raut, V. A. Ganesh, A. S. Nair and S. Ramakrishna, *Energy Environ. Sci.*, 2011, **3**, 3779–3804.
3. G. S. Lim, H. Kim and J. Y. Chang, *J. Mater. Chem. C*, 2014, **2**, 10184–10188.
4. D. G. Chen, *Solar Energy Mater Solar Cells*, 2001, **68**, 313–336.
5. W. Joo, H. J. Kim and J. K. Kim, *Langmuir*, 2010, **26**, 5110–5114.
6. Y. Liu, T. Lai, H. Li, Y. Wang, Z. Mei, H. Liang, Z. Li, F. Zhang, W. Wang, A. Y. Kuznetsov and X. Du, *Small*, 2012, **8** (9), 1392–1397.
7. B. Daglar, T. Khudiyev, G. B. Demirel, F. Buyukserin and M. Bayindir, *J. Mater. Chem. C*, 2013, **1**, 7842–7848.
8. X. Li, J. Gao, L. Xue and Y. Han, *Adv. Funct. Mater.*, 2010, **20**, 259–265.
9. A. Yildirim, T. Khudiyev, B. Daglar, H. Budunoglu, A. K. Okyay and M. Bayindir, *ACS Appl. Mater. Interfaces*, 2013, **5**, 853–860.
10. P. B. Clapham and M. C. Hutley, *Nature*, 1973, **244**, 281–282.
11. J. Nishii, K. Kintaka, Y. Kawamoto, A. Mizutani and H. Kikuta, *J. Ceram. Soc. Jpn.*, 2003, **111**, 24–27.

12. Y. Li, J. Zhang, S. Zhu, H. Dong, F. Jia, Z. Wang, Z. Sun, L. Zhang, Y. Li, H. Li, X. Xu and B. Yang, *Adv. Mater.*, 2009, **21**, 4731–4734.
13. Y. Li, J. Zhang and B. Yang, *Nano Today*, 2010, **5**, 117–127.
14. S. Chattopadhyay, Y. F. Huang, Y. J. Jen, A. Ganguly, K. H. Chen and L. C. Chen, *Materials Science and Engineering R*, 2010, **69**, 1–35.
15. H. Deniz, T. Khudiyev, F. Buyukserin and M. Bayindir, *Appl. Phys. Lett.*, 2011, **99**, 183107.
16. S. Kim, U. T. Jung, S. -K. Kim, J. -H. Lee, H. S. Choi, C. -S. Kim and M. Y. Jeong, *ACS Appl. Mater. Interfaces*, 2015, **7**, 326–331.
17. B. G. Prevo, Y. Hwang and O. D. Velev, *Chem. Mater.*, 2005, **17**, 3642–3651.
18. Y. Hoshikawa, H. Yabe, A. Nomura, T. Yamaki, A. Shimojima and T. Okubo, *Chem. Mater.*, 2010, **22**, 12–14.
19. H. Budunoglu, A. Yildirim and M. Bayindir, *J. Mater. Chem.*, 2012, **22**, 9671–9677.
20. K. Katagiri, S. Yamazaki, K. Inumaru and K. Koumoto, *Polymer Journal*, 2015, **47**, 190–194.
21. J. Moghal, J. Kobler, J. Sauer, J. Best, M. Gardener, A.A.R. Watt and G. Wakefield, *ACS Appl. Mater. Interfaces*, 2012, **4**, 854–859.
22. J. A. Hiller, J. D. Mendelsohn and M. F. Rubner, *Nat. Mater.*, 2002, **1**, 59–63.
23. S. Kim, J. Cho and K. Char, *Langmuir*, 2007, **23**, 6737–6743.
24. Y. Du, L. E. Luna, W. S. Tan, M. F. Rubner and R. E. Cohen, *ACS Nano*, 2010, **4**, 4308–4316.
25. C.G. Bernhard, *Endeavour*, 1967, **26**, 79–84.
26. E. F. Hare, E. G. Shafrn and W. A. Zisman, *J. Phys. Chem.*, 1954, **58**, 236–239.
27. E. G. Shafrin and W. A. Zisman, *J. Phys. Chem.*, 1960, **64**, 519–524.
28. W. A. Zisman, *Advances in Chemistry American Chemical Society: Washington, DC*, 1964.
29. T. Shimogaki, H. Tokoro, M. Tabuchi, N. Koike, Y. Yamashina and M. Takahashi, *J. Sol-Gel Sci. Technol.*, 2015, **74**, 109–113.
30. T. Shimogaki, H. Tokoro, M. Tabuchi, N. Koike, Y. Yamashina and M. Takahashi, *J. Sol-Gel Sci. Technol.*, 2015, **76**, 156–163.
31. T. Shimogaki, H. Tokoro, M. Tabuchi, N. Koike, Y. Yamashina and M. Takahashi, *J. Sol-Gel*

Sci. Technol., 2016, in press.

32. http://www.shinetsusilicone-global.com/products/type/silane/detail/k/co_pro.html

Chapter 6

Conclusion

The present thesis deals with the synthesis of monodispersed porous silica nano-particles and antireflective (AR) coating using porous silica particles.

In Chapter 2, monodispersed porous silica particles with diameters of ca. 100 nm were prepared in high yield. The simultaneous injection of tetramethoxy orthosilicate (TMOS) and n-dodecylamine (DDA) achieved the concentration of the substances constant to keep the reaction rate throughout the preparation process. The gradual supplement of TMOS is important for controlling the particle morphology because the dilute TMOS concentration suppresses silica particle aggregation. The diameters of the microporous silica particles were 100–130 nm. The narrow size distribution resulted from larger particles experiencing smaller growth rates, despite the continuous nucleation occurring during TMOS injection. This method is also applicable for synthesizing smaller silica particles using other template molecules.

In Chapter 3, microporous silica particles of 20–200 nm in particle diameter and 100–1000 m²/g in specific surface area (SSA) were synthesized by the gradual injection of reagents into the reaction system. Increasing the amount of DDA and shortening the DDA injection time yielded particles with larger diameters and SSA values, which also caused aggregation. Adjusting the DDA amount allowed the SSA to be tuned from 100 to 500 m²/g without changing the particle size. The most important parameters for controlling the particle size are the amounts of water and catalyst. It is found that the microporous silica with various morphologies can be obtained by optimizing chemistry and kinetics of the present method.

In Chapter 4, the effect of template molecules on the particle morphology of monodispersed and microporous silica particles via gradual injection of reactants was investigated. Ammonium salts were found to be useful for synthesizing porous silica with a larger SSA value because of their strong interaction with silica species. The use of primary amines is a key to controlling the porosity and morphology. Furthermore, the use of amines with a good solubility in the reaction solution ($\log P_{ow} < 7$) enables the preparation of monodispersed silica particles with diameters of 100 nm whose SSA can be tuned in the range of 40–530 m²/g.

Among such amines, the use of n-decylamine as a templating agent is effective for the synthesis of monodispersed silica particles 100 nm in diameter and 500 m²/g in SSA. These results indicate that the present synthesis method is suitable for the large-scale synthesis of monodispersed and microporous silica particles with a variety of SSAs.

In Chapter 5, a single step fabrication of AR polymer hard coating was achieved. The porous silica particles of 100 nm diameter with surfaces modified by hexamethyldisilazane (HMDS) can segregate spontaneously at the air surface to form a monolayer. The obtained hard-coating film shows AR properties. In this film, the monolayer of porous silica particles can form a low-refractive index layer. HMDS was found to be an effective modifier to control the segregation of the particles at the air surface. One of the advantages of the present approach is that fluorinated modifier is no longer required to adjust the surface energies. A reflectance of 2.7 % and pencil hardness of >H on a PET substrate were achieved. Another advantage is that the silica monolayer can serve as a low-refractive index 100-nm layer. The present approach offers an easier and simpler method for fabricating a robust AR coating for a variety of applications.

From the present thesis, the monodispersed porous silica particle with 100 nm in diameter can be synthesized with high yield by gradual injection method. Using this method, I succeeded in preparation of micro porous silica particles with high monodispersibility and high porosity. The porous silica particles modified with HMDS can segregate spontaneously at the air surface to form a monolayer. This phenomenon can be applied for AR coating which can form easily and exhibit superior mechanical property. This coating system can be applied for other applications by substituting silica particles for others to obtain coating materials with different surface properties. I expect that this system become a new technique to attain new functionalities to coating materials.

List of Publications

1. “Large-Scale Synthesis of Monodisperse Microporous Silica Nanoparticles by Gradual Injection of Reactants”
T. Shimogaki, H. Tokoro, M. Tabuchi, N. Koike, Y. Yamashina and M. Takahashi
Journal of Sol-Gel Science and Technology, 2015, 74, 109–113.
(Chapter 2)
2. “Morphology Control of Microporous Silica Particles Obtained by Gradual Injection of Reactants”
T. Shimogaki, H. Tokoro, M. Tabuchi, N. Koike, Y. Yamashina and M. Takahashi
Journal of Sol-Gel Science and Technology, 2015, 76, 156–163.
(Chapter 3)
3. “Large-Scale Preparation of Morphology-Controlled Microporous Silica Particles via Gradual Injection of Reactants with Different Surfactants”
T. Shimogaki, H. Tokoro, M. Tabuchi, N. Koike, Y. Yamashina and M. Takahashi
Journal of Sol-Gel Science and Technology, 2016, in press.
(Chapter 4)
4. “Single-Process Fabrication of Antireflective Acrylic Hard Coating via Surface Segregation of Porous Silica Nanoparticles”
T. Shimogaki, H. Tokoro, M. Tabuchi, M. Inoue, T. Tsukamoto, T. Ishii, N. Koike, Y. Yamashina and M. Takahashi
RSC advances, 2015, 5, 104792–104797.
(Chapter 5)

Acknowledgment

The work in this thesis was carried out from 2013 to 2016, under the direction of Professor Masahide Takahashi at Department of Materials Science, Graduate School of Engineering, Osaka Prefecture University. The author is sincerely grateful to him for his kind direction and cordial consistent encouragement throughout this work.

Special thanks also to Professor Atsushi Nakahira and Professor Masaya Matsuoka for their insightful comments and suggestions in this thesis.

The author wishes to thank to Mr. Yohzoh Yamashina, Mr. Nobuyuki Koike, Mr. Minoru Tabuchi, Mr. Hiroki Tokoro, Mr. Takuji Tsukamoto and Mr. Masato Inoue for their helpful suggestion and encouragement.

I am particularly grateful for the assistance given by Mr. Tetsuro Agawa, Mr. Hiroshi Hujita, Mr. Nobuyoshi Shirai and Mr. Kiyohumi Takano of DIC Corporation.

I have greatly benefited from Mr. Masahiko Asada, Mr. Hiroshi Maki, Mr. Junichiro Koike and Mr. Toru Ishii of Advanced Evaluation Analysis Center of DIC Corporation for kindly teaching and discussion about the physical analysis and optical simulation.

Ms. Junko Sano and Mr. Akira Kasai of Analysis Center of DIC Corporation give me constructive comments and warm encouragement.

The author also thanks to the all members of Takahashi's Laboratory of Osaka Prefecture University for their encouragement, useful discussion and kind collaboration.

Hearty thanks are made to Mr. Teruki Kiyohara and all members of Polymer Technical Group 10 of DIC Corporation.

Finally, the author wishes to thanks her husband, daughter, parents, brothers and grandparents from the bottom of her heart for their cordial encouragement.

February, 2016

Tomoyo Shimogaki